

## Interdimensional effects in a three-dimensional electron gas with a Rashba spin-orbit coupling interface

A. C. Zulkoskey<sup>⊙,\*</sup>, R. Dick<sup>⊙,†</sup> and K. Tanaka<sup>‡</sup>

*Department of Physics and Engineering Physics, and Centre for Quantum Topology and Its Applications (quanTA),  
University of Saskatchewan, 116 Science Place, Saskatoon, Saskatchewan, Canada S7N 5E2*



(Received 25 November 2019; revised manuscript received 17 March 2020; accepted 13 May 2020;  
published 1 June 2020)

We examine the bound-state and free-state contributions to the density of states in a three-dimensional electron gas with a two-dimensional interface or quantum well with Rashba spin-orbit coupling. The motivation for our research comes from the interest in materials that exhibit Rashba spin splitting of energy bands and the Edelstein and inverse Edelstein effects in quantum wells or interfaces. By modifying the Hamiltonian of three-dimensional electron gas models to include a two-dimensional component with Rashba spin-orbit coupling, we are able to calculate the bound-state and free-state wave functions and corresponding densities of states analytically. In the case of weak asymmetry across the interface, we find that one of the spin-split energy bands has an upper bound where it merges into a three-dimensional energy band. On the other hand, with strong asymmetry across the interface, only one spin-momentum-locked band exists as an interface energy band, which emerges from a three-dimensional energy band.

DOI: [10.1103/PhysRevB.101.235401](https://doi.org/10.1103/PhysRevB.101.235401)

### I. INTRODUCTION

The propagation properties of particles (or quasiparticles) affected by the presence of a surface or an interface in a three-dimensional material can be described using low-dimensional quantum mechanics. Analytic models can be constructed to include extra substructure terms, which affect propagation properties of electrons through a change in the effective mass [1] or confinement in the form of a quantum well [2]. In both cases, the Hamiltonian is constructed as a linear superposition of a free three-dimensional electron gas and a low-dimensional substructure contribution describing the effects of a surface or an interface. The density of states inside the low-dimensional structure that allows for calculation of, e.g., the number of charge carriers and thermal conductivity can be obtained analytically for these types of Hamiltonians, thus providing a powerful tool for studying the interdimensional properties of electrons in a material with substructure.

The system of a two-dimensional (2D) thin quantum well or an attractive interface immersed in a three-dimensional (3D) bulk is described by the Hamiltonian [2],

$$H = \frac{\mathbf{p}^2}{2m} - \mathcal{W}\delta(z - z_0), \quad (1)$$

for a particle of mass  $m$  and  $\mathcal{W} > 0$ . A quantum well of width  $a$  can be considered as thin if  $a \ll \hbar/\sqrt{mk_B T}$  at a given

temperature  $T$ , where  $k_B$  is the Boltzmann constant, as only the lowest subband in the quantum well will be populated, with the thermal wavelength  $\lambda > 2a$ . The Hamiltonian (1) can also be considered as a Kronig-Penney-type approximation of an atomic layer.

The attractive potential yields bound states  $\psi(\mathbf{x}) = \sqrt{\kappa} \exp(i\mathbf{k}_{\parallel} \cdot \mathbf{x}_{\parallel} - \kappa|z - z_0|)/2\pi$ ,  $E = (\hbar^2 \mathbf{k}_{\parallel}^2/2m) - B$ , with the maximum binding energy  $B = \hbar^2 \kappa^2/2m = m\mathcal{W}^2/2\hbar^2$ . There are also states  $\psi(\mathbf{x}) = (2\pi)^{-1} \exp(i\mathbf{k}_{\parallel} \cdot \mathbf{x}_{\parallel})\psi_{k,\pm}(z)$  that move freely across the interface and are relevant for modeling of interfaces through the Hamiltonian (1). The factors  $\psi_{k,\pm}(z)$  and the completeness relation for the eigenstates of (1) can be found in Sec. 3.3 in Ref. [3]. The corresponding density of states (DOS) per volume at the location of the quantum-well structure ( $z = z_0$ ) is given as a function of energy  $E$  by

$$\varrho(E, z_0) = \kappa \varrho_{d=2}(E + (\hbar^2 \kappa^2/2m)) + \varrho_{d=3}(E) \times \left[ 1 - \frac{\hbar\kappa}{\sqrt{2mE}} \arctan\left(\frac{\sqrt{2mE}}{\hbar\kappa}\right) \right], \quad (2)$$

where

$$\varrho_d(E) = 2\Theta(E) \sqrt{\frac{m}{2\pi}} \frac{\sqrt{E}^{d-2}}{\Gamma(d/2)\hbar^d} \quad (3)$$

is the DOS for a free particle of mass  $m$  in  $d$  spatial dimensions and the particle is assumed to have spin 1/2. Integrating the DOS  $\varrho(E, z_0)$  over energy yields the relation between the Fermi energy and the particle density inside the quantum well

\*Corresponding author: [acz621@mail.usask.ca](mailto:acz621@mail.usask.ca)

†[rainer.dick@usask.ca](mailto:rainer.dick@usask.ca)

‡[kat221@campus.usask.ca](mailto:kat221@campus.usask.ca)

at zero temperature [2]:

$$n(z_0)|_{-B < E_F < 0} = \frac{\kappa m}{\pi \hbar^2} \left( E_F + \frac{\hbar^2 \kappa^2}{2m} \right) = \kappa n_2|_{E_{2,F} = K_{2,F}},$$

$$n(z_0)|_{E_F > 0} = \frac{\kappa}{2\pi^2 \hbar^2} \left[ \hbar \kappa \sqrt{2mE_F} - (\hbar^2 \kappa^2 + 2mE_F) \arctan \left( \frac{\sqrt{2mE_F}}{\hbar \kappa} \right) \right] + \frac{\kappa m}{\pi \hbar^2} \left( E_F + \frac{\hbar^2 \kappa^2}{2m} \right) + \frac{1}{3\pi^2} \left( \frac{\sqrt{2mE_F}}{\hbar} \right)^3, \quad (4)$$

where

$$n_d = \frac{2}{\hbar^d \Gamma((d+2)/2)} \sqrt{\frac{mE_F}{2\pi}} \quad (5)$$

is the density of particles in  $d$  spatial dimensions, and  $K_{2,F} = E_F + \hbar^2 \kappa^2 / 2m$  is the kinetic energy inside the quantum well. The analytic results for the DOS and the particle density inside the quantum well smoothly transition from 2D to 3D behavior as the inverse penetration depth  $\kappa = m\mathcal{V}/\hbar^2$  of the bound states approaches zero. Both results demonstrate that bound states exist for  $E \geq -B$ , and that particles confined to the quantum well contribute a 2D density term, made dimensionally correct through the factor  $\kappa$ , reflecting the 3D nature of the system.

Rashba spin-orbit coupling (RSOC) arises as a result of structural inversion asymmetry [4–6]. The Hamiltonian and dispersion relation for a 2D electron gas with RSOC are given by [6,7]

$$H = \frac{\mathbf{p}_{\parallel}^2}{2m} + \alpha [\boldsymbol{\sigma} \times \mathbf{p}_{\parallel} / \hbar] \cdot \hat{z}, \quad E_{\pm}(k_{\parallel}) = \frac{\hbar^2 k_{\parallel}^2}{2m} \pm \alpha k_{\parallel}, \quad (6)$$

where  $m$  is the effective mass of an electron,  $\alpha = -e\hbar E_z(z)/4m^2 c^2$  is the Rashba coefficient,  $E_z(z)$  is an electric field in the direction  $\hat{z}$  perpendicular to the electron gas,  $\boldsymbol{\sigma} = (\sigma_x, \sigma_y, \sigma_z)$  are the Pauli matrices,  $\mathbf{k}_{\parallel} = (k_x, k_y)$  is the two-dimensional wave vector, and  $k_{\parallel} = |\mathbf{k}_{\parallel}|$ . RSOC causes momentum and spin to be “locked in” such that the  $E_+$  and  $E_-$  branches in Eq. (6) have clockwise and counterclockwise winding of spin, respectively, as one goes around the Fermi surface. In Fig. 1,  $E_{\pm}$  are plotted as a function of  $k_x$  for  $k_y = 0$ , where spin points in either  $+y$  or  $-y$  direction. We assume without loss of generality  $\alpha > 0$  in this paper, since negative  $\alpha$  simply corresponds to reversal of the direction of spin winding in each band and amounts to  $\alpha \rightarrow |\alpha|$  in results for energies and densities of states.

The DOS per area per spin in a 2D electron gas,

$$\varrho(E) = \frac{1}{2\pi} \frac{k_{\parallel}(E)}{|dE/dk_{\parallel}|}, \quad (7)$$

is given for the two spin-split energy bands  $E = E_{\pm}(k_{\parallel})$  in Eq. (6) by [7]

$$\varrho_{\pm}(E) = \frac{m}{2\pi \hbar^2} \left( 1 \mp \frac{1}{\sqrt{1 + (2\hbar^2 E / m\alpha^2)}} \right), \quad E \geq 0,$$

$$\varrho_{-}(E) = \frac{m}{\pi \hbar^2 \sqrt{1 + (2\hbar^2 E / m\alpha^2)}}, \quad E < 0. \quad (8)$$

Recent efforts have been put forth in the area of spintronics, which utilizes the spin degree of freedom for information

storage and processing [8]. In candidate materials for spintronics, RSOC induces novel properties in interfaces [9], quantum wells [10–13], and surface quantum wells [14,15]. These properties include the Edelstein effect [16] or the inverse Edelstein effect, where conversion between charge and spin currents occurs [9,17]. To study the effects of a 2D electron gas with RSOC embedded in a 3D system, we discuss Hamiltonians which are a linear combination of 3D kinetic terms and a RSOC term. Materials which necessitate this description include topological insulators [18], interfaces between metallic layers, e.g., Bi/Ag [19,20] or Cu/Bi [21] interfaces, and conducting interfaces between  $\text{LaAlO}_3/\text{SrTiO}_3$  insulating oxide layers [22]. Heterostructures involving metal-oxide interfaces [23] as well as graphene [24,25], in which RSOC is enhanced by proximity to, e.g., transition metal dichalcogenides [9,17], also present systems where RSOC is prominent in 2D substructure within 3D materials.

The remaining sections are laid out as follows. In Sec. II, we calculate the bound-state and free-state wave functions of a symmetric interdimensional model. The cutoff of the inner energy band of interface states is discussed in Sec. III. We present analytic results for the bound-state and free-state density of states for the symmetric model in Sec. IV. In Secs. V and VI, we generalize our results to a surface or an asymmetric interface with different potentials above and below the interface. In particular, Sec. VID also presents results for systems with only a potential step across the interface

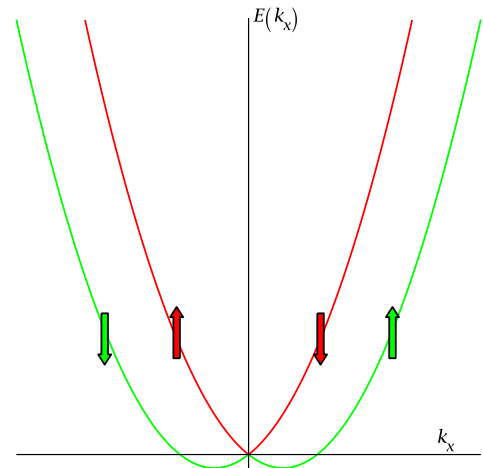


FIG. 1. The spin-split dispersion relation for a 2D electron gas with RSOC for  $k_y = 0$  in arbitrary units. The red (green) curve corresponds to  $E_+$  ( $E_-$ ) in Eq. (6) with a minimum energy of  $E_{\min} = -m\alpha^2/2\hbar^2$ . Up and down arrows correspond to  $+y$  and  $-y$  spin alignment for  $k_y = 0$ .

and no confining potential in the interface. Our findings are summarized in Sec. VII.

## II. INTERDIMENSIONAL EFFECTS OF ELECTRONS WITH RSOC INTERFACE

Motivated by materials which exhibit novel features in interfaces or surfaces as a result of RSOC, as well as heterostructures where RSOC in the interface is enhanced by the neighboring substrate [9,17], we construct a Hamiltonian as a superposition of a 3D free electron gas and a 2D interface or quantum well with RSOC at  $z = z_0$ . Namely, we extend the work of Ref. [1] to include an RSOC term [6] in the interface,

$$H_{\text{SO}} = \alpha[\boldsymbol{\sigma} \times \mathbf{k}_{\parallel}] \cdot \hat{\mathbf{z}}. \quad (9)$$

This yields the second-quantized Hamiltonian,

$$\begin{aligned} H = & \int d^3\mathbf{x} \frac{\hbar^2}{2m} \nabla \psi^\dagger(\mathbf{x}) \cdot \nabla \psi(\mathbf{x}) \\ & - L_{\perp} \int d^2\mathbf{x}_{\parallel} (i\alpha \psi^\dagger(\mathbf{x}_{\parallel}, z_0) (\boldsymbol{\sigma}_{\parallel} \times \nabla_{\parallel}) \cdot \hat{\mathbf{z}} \psi(\mathbf{x}_{\parallel}, z_0) \\ & + V_0 \psi^\dagger(\mathbf{x}_{\parallel}, z_0) \cdot \psi(\mathbf{x}_{\parallel}, z_0)), \end{aligned} \quad (10)$$

where  $\mathbf{x} = (\mathbf{x}_{\parallel}, z)$  and  $\boldsymbol{\sigma}_{\parallel} = (\sigma_x, \sigma_y)$ . The Hamiltonian yields energy expectation values and matrix elements for single-particle wave functions, say,  $\psi_{\mathbf{k}}(\mathbf{x})$  through evaluation of matrix elements between second-quantized states  $|\psi_{\mathbf{k}}\rangle = \int d^3\mathbf{x} \psi^\dagger(\mathbf{x})|0\rangle\psi_{\mathbf{k}}(\mathbf{x})$ . Reported quantum well depths are about 400 meV, e.g., in semiconductor heterostructures [10,11] and in surface quantum wells in PtSe<sub>2</sub> with a submonolayer of rubidium atoms deposited on the surface [15]. Widths vary from 2 nm [13] to about 12.5 nm [11] in semiconductor heterostructures, and can be about 1 nm in surface quantum wells [15]. The  $\delta$ -function approximation is applicable to these systems since the excitation and ionization energies far exceed the thermal energy  $k_B T \simeq 25$  meV at room temperature. For example, the InAs quantum well probed in Ref. [11] with  $m \simeq 0.038 m_e$  would host two energy levels separated by an excitation energy of about 190 meV, so that only the lowest quantum-well state is populated at room temperature. For thin quantum wells of width  $a$  and depth  $V$ , the model parameter  $\mathcal{W} \equiv V_0 L_{\perp}$  in the Hamiltonian in Eq. (10) is roughly equivalent to  $Va$ , but it would be naive to assume the direct analogy,  $V_0 = V$  and  $L_{\perp} = a$ . We are primarily interested in exploring the consequences of a 2D electron gas with RSOC embedded in a bulk, but the model (10) would certainly be too simple to serve as a first-principles microscopic model for real materials. Like the RSOC constant  $\alpha$ , the quantum-well parameter  $\mathcal{W}$  is to be considered as a fitting parameter for using the model to capture quantitative features of 2D RSOC substructure in 3D systems.

Inversion asymmetry that results in RSOC can arise from proximity to a surface in a 3D material, which results in a slight bending of the potential inside the quantum well [11], or due to different atomic layers above and below the conduction plane as in, e.g., BiTeI [26,27] and YBCO [28,29]. Bulk quantum wells and interfaces which are weakly polarized by such proximity effects can be modeled by the Hamiltonian (10) to gain insight into bulk effects on the local density of states. In particular, we find below a cutoff energy for the

inner Rashba cone in the spin-momentum-locked dispersion relation. On the other hand, surfaces and systems with more pronounced asymmetry across substructure will require asymmetric models where the bulk properties above and below the 2D electron gas are different. Furthermore, the assumption of an attractive (or repulsive,  $V_0 < 0$ ) interface potential is not suitable for metal-metal interfaces, which may exhibit RSOC due to the dipolar field built up across the interface. We therefore generalize the Hamiltonian (10) for such systems with strong asymmetry in Sec. V and confirm that a cutoff energy for the inner cone also exists in asymmetric systems as long as asymmetry is not too large. We also find complete suppression of the subdominant interface energy band and partial suppression of the dominant energy band of interface states in the presence of large asymmetry.

The single-particle eigenvalues and eigenfunctions of the Hamiltonian in Eq. (10) are separated into states which are bound to the interface ( $E < \hbar^2 k_{\parallel}^2 / 2m$ ) and free states ( $E \geq \hbar^2 k_{\parallel}^2 / 2m$ ).

The bound states are with  $\kappa \equiv \kappa_{\pm} > 0$  (we set  $z_0 = 0$ ):

$$\begin{aligned} \psi_{\mathbf{k}_{\parallel}, \kappa_{\pm}}(\mathbf{x}_{\parallel}, z) &= \langle \mathbf{x}_{\parallel}, z | \mathbf{k}_{\parallel}, \kappa_{\pm} \rangle \\ &= \frac{\exp(i\mathbf{k}_{\parallel} \cdot \mathbf{x}_{\parallel})}{2\pi} \sqrt{\kappa_{\pm}} \exp(-\kappa_{\pm}|z|) \varphi_{\pm}(\mathbf{k}_{\parallel}), \end{aligned} \quad (11)$$

$$E_{\pm} = \frac{\hbar^2}{2m} (\mathbf{k}_{\parallel}^2 - \kappa_{\pm}^2) = \frac{\hbar^2 k_{\parallel}^2}{2m} - \frac{m L_{\perp}^2}{2\hbar^2} (V_0 \pm \alpha k_{\parallel})^2, \quad (12)$$

where

$$\varphi_{\pm}(\mathbf{k}_{\parallel}) = \frac{1}{\sqrt{2}} \begin{pmatrix} 1 \\ \pm i k_{+} / k_{\parallel} \end{pmatrix}, \quad (13)$$

$k_{\pm} = k_x \pm i k_y$ , and

$$\kappa_{\pm} = (m L_{\perp} / \hbar^2) (V_0 \pm \alpha k_{\parallel}). \quad (14)$$

The free states consist of two sets of even (+) and odd (−) parity eigenstates ( $k_{\perp} \geq 0$ ,  $E = \hbar^2 (\mathbf{k}_{\parallel}^2 + k_{\perp}^2) / 2m$ ),

$$\begin{aligned} \psi_{\mathbf{k}_{\parallel}, k_{\perp}, +}(\mathbf{x}_{\parallel}, z)_{\pm} &= \langle \mathbf{x}_{\parallel}, z | \mathbf{k}_{\parallel}, k_{\perp}, + \rangle_{\pm} \\ &= \frac{\exp(i\mathbf{k}_{\parallel} \cdot \mathbf{x}_{\parallel})}{2\sqrt{\pi^3} \sqrt{1 + (m L_{\perp} / \hbar^2 k_{\perp})^2 (V_0 \pm \alpha k_{\parallel})^2}} \varphi_{\pm}(\mathbf{k}_{\parallel}) \\ &\quad \times \left( \cos(k_{\perp} z) - \frac{m L_{\perp}}{\hbar^2 k_{\perp}} (V_0 \pm \alpha k_{\parallel}) \sin(k_{\perp} |z|) \right), \end{aligned} \quad (15)$$

$$\begin{aligned} \psi_{\mathbf{k}_{\parallel}, k_{\perp}, -}(\mathbf{x}_{\parallel}, z)_{\pm} &= \langle \mathbf{x}_{\parallel}, z | \mathbf{k}_{\parallel}, k_{\perp}, - \rangle_{\pm} \\ &= \frac{\exp(i\mathbf{k}_{\parallel} \cdot \mathbf{x}_{\parallel})}{2\sqrt{\pi^3}} \sin(k_{\perp} z) \varphi_{\pm}(\mathbf{k}_{\parallel}). \end{aligned} \quad (16)$$

We could have used any 2-spinor basis  $\varphi_s$  for representation of the odd states in Eq. (16), since they are not affected by RSOC. We use the chiral spin-momentum-locked basis  $\varphi_{\pm}(\mathbf{k}_{\parallel})$  also for these states for convenience.

The spinors  $\varphi_{\pm}(\mathbf{k}_{\parallel})$  satisfy the eigenvalue equation,

$$(\mathbf{k}_{\parallel} \times \boldsymbol{\sigma}) \cdot \varphi_{\pm}(\mathbf{k}_{\parallel}) = \pm \hat{\mathbf{z}} k_{\parallel} \varphi_{\pm}(\mathbf{k}_{\parallel}). \quad (17)$$

Namely,  $\varphi_+(\mathbf{k}_\parallel)$  yields mathematically positive (counterclockwise) spin orientation along a 2D Fermi surface  $k_\parallel = \text{const.}$  in the  $k_x k_y$  plane, while  $\varphi_-(\mathbf{k}_\parallel)$  yields mathematically negative (clockwise) spin orientation. We thus call  $\varphi_+(\mathbf{k}_\parallel)$  and  $\varphi_-(\mathbf{k}_\parallel)$  the right- and left-chiral spinors, respectively.

Note that the bound states in the interface in Eq. (11) have even parity. We call these states *interface states* in the following for consistency with the notation used in Sec. V, where we also encounter states that are bound in the bulk region on one side of the interface. In order for the ground-state energy to exist as a lower bound in Eq. (12), we require

$$\eta^2 \leq 1, \quad (18)$$

where  $\eta = m\alpha L_\perp/\hbar^2$ . Without this restriction  $E \rightarrow -\infty$  as  $k_\parallel \rightarrow \infty$ . The restriction (18) will always be fulfilled in 2D systems that we propose to model with the Hamiltonian in Eq. (10). Equation (18) implies

$$L_\perp \leq \frac{\hbar^2}{m\alpha} = 832 \text{ nm} \quad (19)$$

for the values  $\alpha = 2.41 \times 10^{-3} \text{ eV nm}$  and  $m = 0.038 m_e$  observed in InAs quantum wells [10]. This upper bound is much larger than, e.g., the width 12.5 nm of the InAs quantum well studied in Ref. [11]. Moreover,

$$L_\perp \leq \frac{\hbar^2}{m\alpha} \simeq 2 \text{ nm} \quad (20)$$

for the values  $\alpha = 0.385 \text{ eV nm}$  and  $m \simeq 0.1 m_e$  observed in BiTeI [26]. This upper bound is still much larger than the separation  $\lesssim 0.2 \text{ nm}$  between the atomic layers in BiTeI.

For interpretation of the constraint (18), we note that  $v_R = \alpha/\hbar$  corresponds to a velocity. This ‘‘Rashba velocity’’ impacts the motion of particles in the RSOC interface or quantum well through

$$v_{\parallel,\pm} = \frac{1}{\hbar} \frac{\partial E_\pm}{\partial k_\parallel} = \frac{\hbar k_\parallel}{m} \pm v_R \hat{k}_\parallel. \quad (21)$$

The condition (18) then states that the shift in the kinetic momenta  $mv_{\parallel,\pm}$  due to RSOC should not resolve the effective width  $L_\perp$  of the interface or quantum well,

$$mv_R \leq \hbar/L_\perp. \quad (22)$$

The Hamiltonian in Eq. (10) yields the dispersion relation in Eq. (12),

$$E = E(|\mathbf{k}_\parallel|, \kappa_\pm) \equiv E_\pm(k_\parallel), \quad (23)$$

for the interface states  $|\mathbf{k}_\parallel, \kappa_\pm\rangle$  with  $E < \hbar^2 k_\parallel^2/2m$ , and

$$E = E(|\mathbf{k}_\parallel|, k_\perp) = \frac{\hbar^2}{2m} (k_\parallel^2 + k_\perp^2) \quad (24)$$

for the free states  $|\mathbf{k}_\parallel, k_\perp, \pm\rangle_\pm$  with  $E \geq \hbar^2 k_\parallel^2/2m$ . The corresponding DOS is given by [1]

$$\begin{aligned} \varrho(E, \mathbf{x}) = & \sum_{\pm} \int d^2 \mathbf{k}_\parallel \left( \delta(E - E_\pm(k_\parallel)) |\langle \mathbf{x} | \mathbf{k}_\parallel, \kappa_\pm \rangle|^2 \right. \\ & \left. + \Theta(E - \hbar^2 k_\parallel^2/2m) \left| \frac{\partial k_\perp(E, \mathbf{k}_\parallel)}{\partial E} \right| |\langle \mathbf{x} | \mathbf{k}_\parallel, k_\perp \rangle_\pm|^2 \right), \end{aligned} \quad (25)$$

where the sum over even- and odd-parity free states is implicitly assumed, and as such + and – for parity have been removed from the eigenvectors. Hence,

$$\begin{aligned} \varrho(E, \mathbf{x}) = & \sum_{\pm} \left( \int_0^{2\pi} d\theta k_\parallel \left| \frac{\partial k_\parallel(E_\pm)}{\partial E_\pm} \right|_{E_\pm=E} |\langle \mathbf{x} | \mathbf{k}_\parallel, \kappa_\pm \rangle|^2 \right. \\ & \left. + \int d^2 \mathbf{k}_\parallel \Theta(E - \hbar^2 k_\parallel^2/2m) \right. \\ & \left. \times \left| \frac{\partial k_\perp(E, \mathbf{k}_\parallel)}{\partial E} \right| |\langle \mathbf{x} | \mathbf{k}_\parallel, k_\perp \rangle_\pm|^2 \right). \end{aligned} \quad (26)$$

Note that only the interface states (11) yield the spin-split dispersion relation in Eq. (12). However, for the even-parity free states in Eq. (15), the Rashba term still induces a spin preference for a given momentum  $\mathbf{k}_\parallel + k_\perp \hat{z}$ ,

$$\begin{aligned} & \frac{|\langle \mathbf{x}_\parallel, z | \mathbf{k}_\parallel, k_\perp, + \rangle_+|^2}{|\langle \mathbf{x}_\parallel, z | \mathbf{k}_\parallel, k_\perp, + \rangle_-|^2} \\ &= \frac{1 + (mL_\perp/\hbar^2 k_\perp)^2 (V_0 - \alpha k_\parallel)^2}{1 + (mL_\perp/\hbar^2 k_\perp)^2 (V_0 + \alpha k_\parallel)^2} \\ & \times \frac{(\cos(k_\perp z) - (mL_\perp/\hbar^2 k_\perp)(V_0 + \alpha k_\parallel) \sin(k_\perp |z|))^2}{(\cos(k_\perp z) - (mL_\perp/\hbar^2 k_\perp)(V_0 - \alpha k_\parallel) \sin(k_\perp |z|))^2}. \end{aligned} \quad (27)$$

In particular, the right-chiral free states are suppressed relative to the left-chiral free states in the interface  $z = z_0 \equiv 0$ .

We evaluate different contributions to the DOS in Eq. (26) in the interface in Sec. IV.

### III. DISPERSION RELATION OF INTERFACE STATES AND CUTOFF OF ONE INTERFACE ENERGY BAND

In a purely 2D system with RSOC, an applied electric field along  $+x$  causes electrons to move in the  $-x$  direction and populate states with  $k_x < 0$  at the expense of states with  $k_x > 0$ . Figure 2 illustrates the shift of the inner and outer Fermi circles due to an applied electric field in the  $x$  direction. An increase in  $-y$  and  $+y$  spin polarization states for  $k_y = 0$  creates a net  $-y$  spin polarization, as the outer Fermi circle dominates over the inner one with a larger number of states. This is the well-known Edelstein effect [9,16,17], where a charge current is converted to an accumulation of spin in the transverse direction. Likewise, the inverse Edelstein effect is the conversion of a spin current to a transverse charge current [9,17,19].

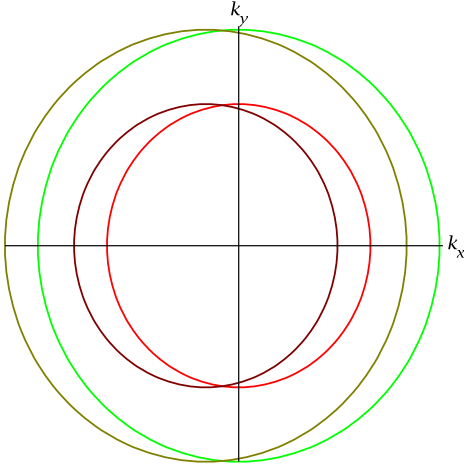


FIG. 2. The shifted Fermi surfaces of a 2D electron gas with RSOC due to an applied electric field in the  $x$  direction. The red (green) circle corresponds to the  $E_+$  ( $E_-$ ) branch for the applied electric field  $\mathbf{E} = 0$  and the maroon (olive) circle corresponds to the  $E_+$  ( $E_-$ ) branch for  $\mathbf{E} \neq 0$ .

In our 3D model we find that the requirement  $\kappa_- > 0$  in Eq. (14) implies  $k_{\parallel} < V_0/\alpha$  in order for an interface state with the left chirality to exist. This restricts the energy  $E_-$  in Eq. (12) to a maximum value of  $E_{-, \max} = \hbar^2 V_0^2 / 2m\alpha^2$ . The spin-split energy bands in Eq. (12), made dimensionless as  $\epsilon_{\pm} = (2mL_{\perp}^2/\hbar^2)E_{\pm}$ , are plotted as a function of  $k_x L_{\perp}$  for  $k_y = 0$  in Figs. 3 and 4. We use the dimensionless parameters,

$$\beta = \frac{mV_0L_{\perp}^2}{\hbar^2} = 0.131 \frac{m}{m_e} \frac{V_0}{\text{eV}} \left( \frac{L_{\perp}}{\text{\AA}} \right)^2, \quad (28)$$

$$\eta = \frac{m\alpha L_{\perp}}{\hbar^2} = 0.131 \frac{m}{m_e} \frac{\alpha}{0.1 \text{ eV nm}} \frac{L_{\perp}}{\text{\AA}}. \quad (29)$$

We use these angstrom-scale width parameters for illustrative purposes because the most interesting aspects of the

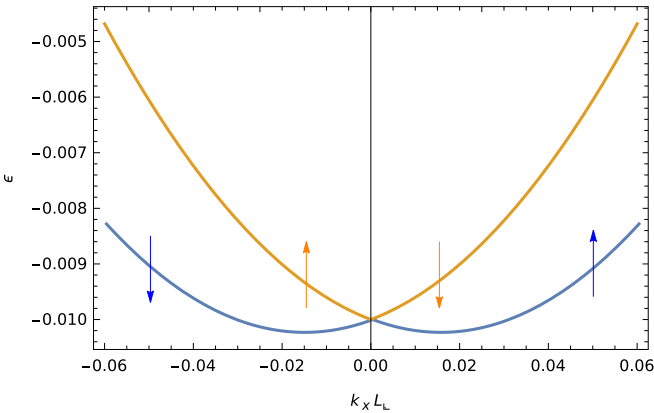


FIG. 3. The spin-split energy bands  $\epsilon_{\pm} = (2mL_{\perp}^2/\hbar^2)E_{\pm}$  of interface states as a function of  $k_x L_{\perp}$  for  $k_y = 0$  and small values of  $k_x L_{\perp}$ . The orange (blue) curve corresponds to  $E_-$  ( $E_+$ ) in Eq. (12) with a minimum dimensionless energy of  $2mE_{\min}L_{\perp}^2/\hbar^2 = -\beta^2/(1-\eta^2)$ . Here,  $\beta = 0.1$  and  $\eta = 0.15$ . The arrows indicate spin projection along the  $y$  axis.

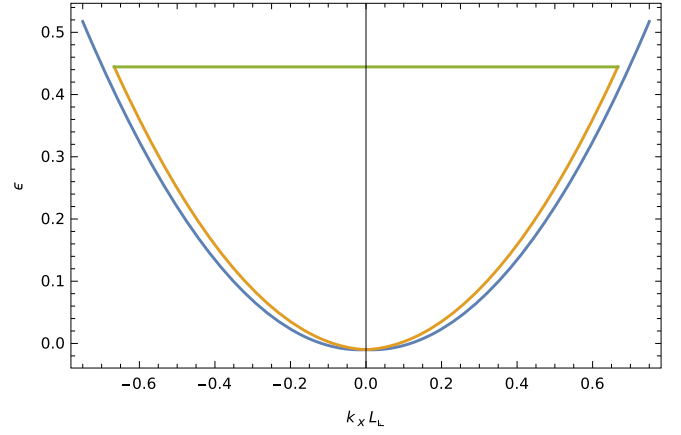


FIG. 4. The spin-split energy bands  $\epsilon_{\pm} = (2mL_{\perp}^2/\hbar^2)E_{\pm}$  of interface states as a function of  $k_x L_{\perp}$  for  $k_y = 0$ . The orange (blue) curve corresponds to  $E_-$  ( $E_+$ ) in Eq. (12). Due to the requirement  $\kappa_- > 0$ ,  $E_-$  is restricted to a maximum dimensionless energy of  $(V_0 L_{\perp}/\alpha)^2 = \beta^2/\eta^2$ . The cutoff is indicated by the green line. Here,  $\beta = 0.1$  and  $\eta = 0.15$ .

model (10) occur within atomic-scale layers. Note from Eq. (12) or Figs. 3 and 4 that  $E_- \geq E_+$  where both branches exist.

As shown below, there is an upper bound  $E_{-, \max}$  on the interface energy band  $E_-(k_{\parallel})$  corresponding to a transition where this band merges into a bulk energy band. The transition energy  $E_{-, \max}$  can be within accessible energy ranges for interfaces or atomic layers with a large denominator  $m\alpha^2$ , e.g., for heavy-fermion systems with giant RSOC. For example, for BiTeI we have  $m \simeq 0.1 m_e$  and  $\alpha = 0.385 \text{ eV nm}$  along atomic layers in the bulk [26]. This yields the upper bound,

$$E_- \lesssim 2.6 \text{ eV} \left( \frac{V_0}{\text{eV}} \right)^2. \quad (30)$$

This might be reduced further for BiTeI surface states where even larger RSOC constants and effective masses have been reported [27], and it would be ideal to have a surface or interface system with a sub-eV limit on  $E_-$ . As emphasized earlier, the strength  $\mathcal{W} = V_0 L_{\perp}$  of the attractive potential is a model parameter to be determined from model fitting rather than from first principles; however,  $V_0$  can be taken as proxy for the binding energies of valence electrons. These are expected to be in the eV energy range for atomic layers within materials, but can also be weaker especially on surfaces and within interfaces. Observation of the transition energy  $E_{-, \max}$  is therefore achievable not only in giant-Rashba heavy-fermion systems, but also in interface or surface systems with weakly bound fermions experiencing strong RSOC.

The possible competition or interplay between interface-bound and free states for the spin-charge correlation in an RSOC interface warrants a more detailed analysis in terms of the corresponding densities of states, as presented in the following section.

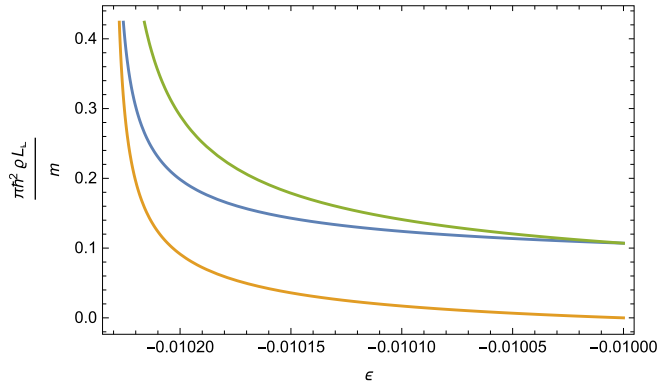


FIG. 5. The DOS in Eq. (31) at  $z = z_0$  for  $E_{\min} \leq E \leq -mV_0^2 L_\perp^2 / 2\hbar^2$  in units of  $m/(\pi \hbar^2 L_\perp)$ . The energy variable is  $\epsilon = 2mEL_\perp^2/\hbar^2$ . Only the  $E_+$  branch contributes in this energy range. The green curve is the total density of interface states, while the blue (orange) curve is the contribution from the + (−) sign choice in the solutions for  $k_\parallel$  in term of  $E_+$ . Parameters are  $\beta = 0.1$  and  $\eta = 0.15$ .

#### IV. DENSITIES OF INTERFACE AND FREE STATES AT $z = z_0$

The restriction on the energy range for the  $E_-$  branch also impacts the density of interface states at  $z = z_0$ . Substituting Eq. (11) in Eq. (26) yields the DOS of the spin-split energy bands in three energy ranges. For  $E_{\min} \equiv -mV_0^2 L_\perp^2 / 2\hbar^2 (1 - \eta^2) \leq E < -mV_0^2 L_\perp^2 / 2\hbar^2$  only the  $E_+$  branch contributes to the DOS:

$$\begin{aligned} \varrho(E, z_0) &= \varrho_+(E, z_0) \\ &= \sum_{(\pm)} \int_0^{2\pi} d\theta k_\parallel \left| \frac{\partial k_\parallel^{(\pm)}(E_+)}{\partial E_+} \right|_{E_+=E} |\langle \mathbf{x}_\parallel, z_0 | \mathbf{k}_\parallel, \kappa_\pm \rangle|^2 \\ &= \frac{m\eta}{\pi \hbar^2 L_\perp} \frac{2\beta^2 + (1 - \eta^2)\epsilon}{(1 - \eta^2)^2 \sqrt{(1 - \eta^2)\epsilon + \beta^2}}, \end{aligned} \quad (31)$$

where  $\beta = mV_0 L_\perp^2 / \hbar^2$ ,  $\eta = m\alpha L_\perp / \hbar^2$ , and  $\epsilon = 2mEL_\perp^2 / \hbar^2$ . The summation  $\sum_{(\pm)}$  above refers to the contributions of the two roots  $k_\parallel^{(\pm)}(E_+)$  for the in-plane momentum as a function of energy in this energy range.

Equation (31) also shows that the DOS for  $E_{\min} \leq E < -mV_0^2 L_\perp^2 / 2\hbar^2$  contains a van Hove singularity [30] at  $E = E_{\min} \Rightarrow \epsilon = \epsilon_{\min} = -\beta^2 / (1 - \eta^2)$ . This singularity occurs at the bottom of the  $E_+$  branch, which is analogous to the van Hove singularity at  $E = -m\alpha^2 / 2\hbar^2$  in the purely 2D model [6]. The two-dimensional results have already demonstrated that the van Hove singularity, through its enhancement of the differential tunneling conductance  $dI/dV$ , can be used to probe the Rashba spin splitting in scanning tunneling spectroscopy [27,31]. The peak in the DOS is also expected to impact the polaronic properties [32,33], superconductivity [29], and the low-energy scattering [34] of electrons in interfaces with RSOC. Shown in Fig. 5 is the DOS in the energy range  $E_{\min} \leq E < -mV_0^2 L_\perp^2 / 2\hbar^2$ .

The densities of interface states for  $E \geq -mV_0^2 L_\perp^2 / 2\hbar^2$  are displayed in Fig. 6 and are given for the two spin-split energy

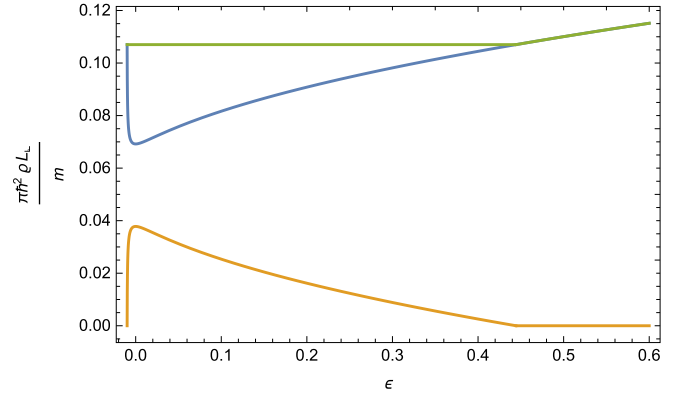


FIG. 6. The spin-split and total DOS at  $z = z_0$  for  $E \geq -mV_0^2 L_\perp^2 / 2\hbar^2$  in units of  $m/(\pi \hbar^2 L_\perp)$ . The energy variable is  $\epsilon = 2mEL_\perp^2/\hbar^2$ . The green curve is the total density of interface states, while the blue and orange curves correspond to, respectively,  $\varrho_+(E, z_0)$  and  $\varrho_-(E, z_0)$  in Eq. (32). Parameters are  $\beta = 0.1$  and  $\eta = 0.15$ .

bands in Eq. (12) by

$$\begin{aligned} \varrho_\pm(E, z_0) &= \int_0^{2\pi} d\theta k_\parallel \left| \frac{\partial k_\parallel(E_\pm)}{\partial E_\pm} \right|_{E_\pm=E} |\langle \mathbf{x}_\parallel, z_0 | \mathbf{k}_\parallel, \kappa_\pm \rangle|^2 \\ &= \frac{m}{2\pi \hbar^2 L_\perp} \frac{\sqrt{\beta^2 + (1 - \eta^2)\epsilon} \pm \eta\beta}{(1 - \eta^2)^2} \\ &\quad \times \frac{\beta \pm \eta\sqrt{\beta^2 + (1 - \eta^2)\epsilon}}{\sqrt{\beta^2 + (1 - \eta^2)\epsilon}} \\ &\quad \times \Theta(E + mV_0^2 L_\perp^2 / 2\hbar^2). \end{aligned} \quad (32)$$

The total density of interface states for  $-mV_0^2 L_\perp^2 / 2\hbar^2 \leq E \leq \hbar^2 V_0^2 / 2m\alpha^2$  is

$$\varrho(E, z_0) = \frac{\beta(1 + \eta^2)}{L_\perp(1 - \eta^2)^2} \varrho_{d=2}(K_2), \quad (33)$$

where  $K_2 = E + mV_0^2 L_\perp^2 / 2\hbar^2$  is the kinetic energy of electrons whose wave functions are exponentially suppressed perpendicular to the interface and  $\varrho_{d=2}(K_2) = \Theta(K_2)m/\pi \hbar^2$  is the DOS of free electrons in two dimensions.

Equation (33) demonstrates that the total DOS in the energy range where both spin-split bands contribute is proportional to the free 2D DOS, scaled by  $L_\perp$  to reflect the 3D nature of the system. For  $E > \hbar^2 V_0^2 / 2m\alpha^2$  the  $E_-$  branch no longer contributes and the bound-state DOS is given by  $\varrho_+(E, z_0)$  in Eq. (32). This is shown in Fig. 6.

The density of free states in the interface has contributions from the right- and left-chiral states with even parity in Eq. (15),

$$\varrho_f(E, z_0) = \varrho_{f+}(E, z_0) + \varrho_{f-}(E, z_0), \quad (34)$$

where

$$\begin{aligned} \varrho_{f\pm}(E, z_0) &= \int d^2 \mathbf{k}_\parallel \Theta(E - \hbar^2 \mathbf{k}_\parallel^2 / 2m) \left| \frac{\partial k_\perp(E, \mathbf{k}_\parallel)}{\partial E} \right| \\ &\quad \times |\langle \mathbf{x} | \mathbf{k}_\parallel, k_\perp \rangle_\pm|^2. \end{aligned} \quad (35)$$

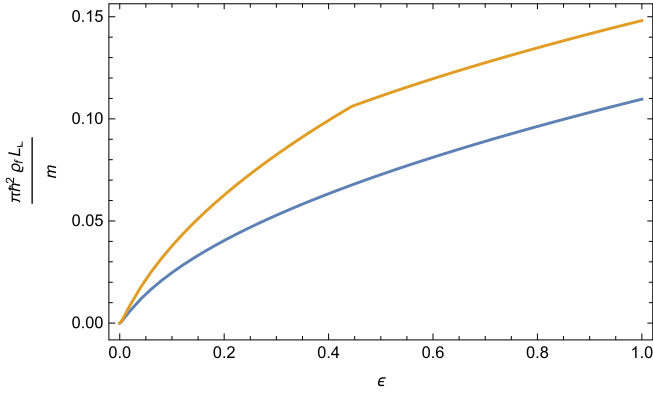


FIG. 7. The spin-split density of free states at  $z = z_0$  in units of  $m/(\pi\hbar^2L_\perp)$ . The blue and orange curves correspond to, respectively,  $\varrho_{f+}(E, z_0)$  and  $\varrho_{f-}(E, z_0)$  in Eq. (37). At  $2mEL_\perp^2/\hbar^2 = \beta^2/\eta^2$ ,  $\varrho_{f-}(E, z_0)$  exhibits a cusp, which is related to the appearance of the interface states in  $\varrho_-(E, z_0)$ , see Fig. 6. Parameters are  $\beta = 0.1$  and  $\eta = 0.15$ .

Substitution of the wave functions leads to

$$\varrho_{f\pm}(E, z_0) = \frac{m\Theta(E)}{2\pi^2\hbar^2L_\perp} \int_0^{\sqrt{2mEL_\perp^2/\hbar}} dx \times \frac{x\sqrt{2mEL_\perp^2/\hbar^2 - x^2}}{2mEL_\perp^2/\hbar^2 - x^2 + (mL_\perp/\hbar^2)^2(V_0L_\perp \pm \alpha x)^2}. \quad (36)$$

Integration then yields

$$\varrho_{f\pm}(E, z_0) = \frac{m\Theta(E)}{2\pi^2\hbar^2L_\perp} \frac{b_\pm(E, \beta, \eta)}{(1 - \eta^2)\sqrt{d(E, \beta, \eta)}} \times \left[ \sqrt{\frac{2mEL_\perp^2}{\hbar^2} - c_\pm(E, \beta, \eta)} \arctan\left(\frac{\sqrt{2mEL_\perp^2/\hbar^2}}{c_\pm(E, \beta, \eta)}\right) \right], \quad (37)$$

where

$$\begin{aligned} d(E, \beta, \eta) &= \beta^2 + \frac{2mEL_\perp^2}{\hbar^2}(1 - \eta^2), \\ b_\pm(E, \beta, \eta) &= \sqrt{d(E, \beta, \eta)} \pm \eta\beta, \\ h_\pm(E, \beta, \eta) &= \left( \frac{\sqrt{d(E, \beta, \eta)} \pm \eta\beta}{1 - \eta^2} \right)^2, \\ c_\pm(E, \beta, \eta) &= \sqrt{h_\pm(E, \beta, \eta) - 2mEL_\perp^2/\hbar^2}. \end{aligned} \quad (38)$$

The spin-split densities of free states in Eq. (37) are presented in Fig. 7. The result for  $\varrho_{f-}(E, z_0)$  contains a cusp at  $2mEL_\perp^2/\hbar^2 = \beta^2/\eta^2$ , which corresponds to  $k_\parallel = V_0/\alpha$ ,  $k_\perp = 0$  and the energy cap on the  $E_-$  branch. This cusp originates in the  $\partial k_\perp/\partial E \sim 1/k_\perp$  term in Eq. (26).  $k_\perp = 0$  does not necessarily generate a critical point in the DOS due to  $|\langle x|\mathbf{k}_\parallel, k_\perp\rangle_\pm|^2$  multiplied to  $|\partial k_\perp/\partial E|$  in Eq. (26), with the wave function given in Eq. (15) vanishing sufficiently quickly.

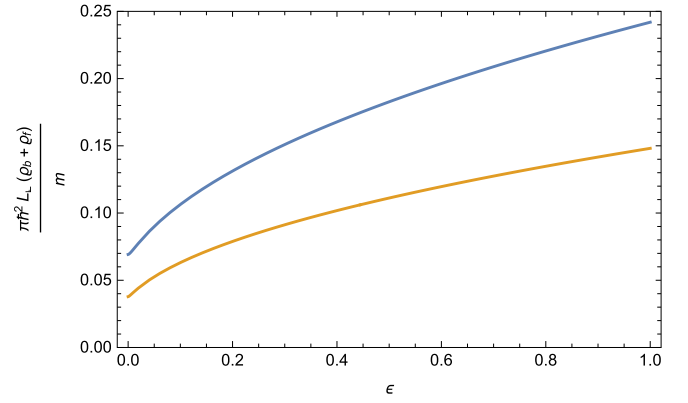


FIG. 8. The spin-split DOS at  $z = z_0$  in units of  $m/(\pi\hbar^2L_\perp)$ . The blue and orange curves correspond to  $\varrho_+(E, z_0) + \varrho_{f+}(E, z_0)$  and  $\varrho_-(E, z_0) + \varrho_{f-}(E, z_0)$ , respectively. Parameters are  $\beta = 0.1$  and  $\eta = 0.15$ .

However, when the interface states cease to exist in the  $E_-$  branch, the  $1/k_\perp$  divergence in the integrand in Eq. (36) for  $\varrho_{f-}(E, z_0)$  is no longer compensated, while the singularity is still integrable. This results in the cusp.

Consistently with the enhancement of the free left-chiral wave functions in the interface in Eq. (27), Fig. 7 shows that the left chirality dominates the contribution from the free states, contrary to the interface bound states in Fig. 6. However, the sum of the free-state and bound-state densities of states still exhibits domination of the right-chiral states in the interface, which is shown in Fig. 8. These figures also demonstrate that the interface states dominate overall in the interface, which means that the “3D+2D” model lends credibility to the 2D model for discussing features of RSOC interfaces.

There is no cusp in the sum  $\varrho_-(E, z_0) + \varrho_{f-}(E, z_0)$  at the energy parameter  $2mEL_\perp^2/\hbar^2 = \beta^2/\eta^2$  where the left-chiral interface states in  $\varrho_-(E, z_0)$  are cut off and the corresponding free-state DOS,  $\varrho_{f-}(E, z_0)$ , has a cusp. For the right-chiral states, we can maintain the distinction between transversally damped interface states in  $\varrho_+(E, z_0)$  and free states in  $\varrho_{f+}(E, z_0)$  throughout the energy ranges where we expect these states to exist. In contrast, for the left-chiral states the interface states (which have the energy cap shown in Fig. 4 from  $\kappa_- > 0$ ) appear like a missing segment of the free states.

Figure 8 shows that the model with 2D RSOC substructure embedded in a 3D bulk as in Eq. (10) still predicts the domination of the right chirality as does the purely 2D model. However, Figs. 6 and 7 also imply that this occurs through a competition of interface and free states. Kinetic transport in a 2D electron gas with combined Rashba and Dresselhaus spin-orbit coupling has been analyzed by Schliemann and Loss [35]. We here use a relaxation time approximation for the 2D isotropic case of pure Rashba coupling. This yields again the electrical conductivity  $\sigma_e = \sigma_{e,+} + \sigma_{e,-}$ , where the contributions from the two oppositely polarized branches are

$$\sigma_{e,\pm} = n_\pm \frac{e^2\tau}{m} = \frac{e^2\tau}{m} \int_{E_{\pm,\min}}^{E_F} dE \varrho(E_\pm, z_0). \quad (39)$$

The net spin current density with spin-polarization  $\alpha\hat{z} \times \hat{E}/|\alpha|$  associated with the electric current density  $\mathbf{j}_e = \sigma_e \mathbf{E}$

TABLE I. States in the potential in Eq. (42).

Case	$\psi(z > 0)$	$\psi(z < 0)$	Energy	Designation and notation for $z$ -dependent factors
I	$\exp(ik_z z), k_z \in \mathbb{R}$	$\exp(\pm ik_i z), k_i > 0$	$E \geq \Phi$	Free states $\langle z k_{\parallel}, k_i, \pm \rangle_f$
II	$\exp(-\kappa z), \kappa > 0$	$\exp(\pm ik_i z), k_i > 0$	$E \geq 0$	Bound states (or semi-free states) $\langle z k_{\parallel}, k_i, \pm \rangle_b$
III	$\exp(-\kappa_{\pm} z), \kappa_{\pm} > 0$	$\exp(-\kappa_{i,\pm} z), \kappa_{i,\pm} > 0$	$E \geq -\hbar^2 \kappa_{i,\pm}^2 / 2m_*$	Interface states $\langle z k_{\parallel}, \pm \rangle$

is then

$$\mathbf{j}_s = -(n_+ - n_-)e\hbar\tau E/2m. \quad (40)$$

There appears an extra minus sign in the spin conductivity,  $\sigma_{s,\pm} = \mp(\hbar/2e)\sigma_{e,\pm}$ , because electrons as the carriers of spin projections  $\pm\hbar/2$  flow in the  $-E$  direction. The extra minus sign would be absent for hole transport. The (inverse) Edelstein effect for in-plane charge-spin correlation is a consequence of

$$n_+(z_0) = \int_{-\hbar^2\beta^2/[2mL_{\perp}^2(1-\eta^2)]}^{E_F} dE(\varrho_+(E, z_0) + \varrho_{f+}(E, z_0))$$

$$> n_-(z_0) = \int_{-\hbar^2\beta^2/2mL_{\perp}^2}^{E_F} dE(\varrho_-(E, z_0) + \varrho_{f-}(E, z_0)), \quad (41)$$

similarly as in the 2D model.

## V. AN ASYMMETRIC MODEL FOR RSOC INTERFACE

The analysis so far has been aided by the assumption of symmetry across a thin interface. However, Rashba spin orbit coupling would naturally occur in an asymmetric setting. Furthermore, the resulting chiral spin structure and related Edelstein effect would usually be observed on surfaces. Therefore, in this section, we analyze the density of states and its impact on the Edelstein effect on a surface or asymmetric interface which is modeled by a step function of height  $\Phi > 0$  combined with an attractive  $\delta$ -function potential and a RSOC term,

$$V(z) = \Theta(z)\Phi - \mathcal{W}\delta(z) + \tilde{\alpha}(\boldsymbol{\sigma} \times \mathbf{p}/\hbar) \cdot \hat{z}\delta(z). \quad (42)$$

In the following, we address systems that can be described by the above potential as an interface for brevity; however, this asymmetric model can also describe surfaces or atomic layers with a skewed potential across the layers due to proximity effects.

In description of a surface in terms of  $V(z)$ , the bulk material is located at  $z < 0$  and the work function for the bulk states would be  $W = \Phi - E_F$ , where  $E_F$  is the Fermi energy. The attractive  $\delta$ -function potential accounts for the possibility of surface states. These states will supply the 2D electron gas that experiences RSOC. The length parameter  $L_{\perp}$  has been absorbed into the RSOC constant,  $\tilde{\alpha} = \alpha L_{\perp}$ .

To make the model as realistic as possible for a surface or an interface connecting two different materials, we also allow for different effective masses,  $m$  and  $m_*$ , on either side of the interface,

$$m(z) = m\Theta(z) + m_*\Theta(-z), \quad (43)$$

for the discussion of interface states. We also continue to assume  $\tilde{\alpha} \geq 0$ , since changing the sign of  $\tilde{\alpha}$  only reverses the direction of chiral spin structure in each band, and all

our analytic results for the corresponding states are swapped between the two bands under  $\tilde{\alpha} \rightarrow -\tilde{\alpha}$ .

The potential in Eq. (42) admits states of the form,

$$\langle \mathbf{x}|\Psi \rangle = \frac{\exp(i\mathbf{k}_{\parallel} \cdot \mathbf{x}_{\parallel})}{2\pi} \varphi_{\pm}(\mathbf{k}_{\parallel}) \psi(z), \quad (44)$$

which can be damped exponentially or propagate freely on either side of the interface. We will use the nomenclature outlined in Table I.

For simplicity, we denote the states in cases II and III as bound states and interface states, respectively, although we have to keep in mind that exponentially suppressed states in the  $z$  direction can elastically scatter into free states if  $E \geq \Phi$ . The designation of the bound states is motivated by modeling of a surface, where case II corresponds to bulk states in the material.

Continuity of  $\exp(-iEt/\hbar)$  relates wave numbers or damping coefficients:

$$\text{I. } E = \Phi + \frac{\hbar^2}{2m}(k_{\parallel}^2 + k_z^2) = \frac{\hbar^2}{2m_*}(k_{\parallel}^2 + k_i^2), \quad (45)$$

$$\text{II. } E = \Phi + \frac{\hbar^2}{2m}(k_{\parallel}^2 - \kappa^2) = \frac{\hbar^2}{2m_*}(k_{\parallel}^2 + k_i^2), \quad (46)$$

$$\text{III. } E = \Phi + \frac{\hbar^2}{2m}(k_{\parallel}^2 - \kappa_{\pm}^2) = \frac{\hbar^2}{2m_*}(k_{\parallel}^2 - \kappa_{i,\pm}^2). \quad (47)$$

For calculation of the states we have taken into account that the Schrödinger equation with a local mass  $m(\mathbf{x})$  is

$$E\Psi(\mathbf{x}) = -\nabla \cdot \frac{\hbar^2}{2m(\mathbf{x})} \cdot \nabla \Psi(\mathbf{x}) + V(\mathbf{x})\Psi(\mathbf{x}). \quad (48)$$

This follows from hermiticity of the Hamiltonian, or equivalently from replacing the mass  $m$  in the Lagrange density of the Schrödinger field,

$$\mathcal{L} = \frac{i\hbar}{2} \left( \Psi^\dagger \frac{\partial \Psi}{\partial t} - \frac{\partial \Psi^\dagger}{\partial t} \Psi \right) - \frac{\hbar^2}{2m} \nabla \Psi^\dagger \cdot \nabla \Psi - \Psi^\dagger V \Psi, \quad (49)$$

with a local mass  $m(\mathbf{x})$ . In case of a change of mass from the effective mass  $m_*$  inside to  $m$  outside of the interface, this replaces the smoothness condition for  $\psi(z)$  across the step with the continuity condition,

$$\psi(0 + \epsilon) = \psi(0 - \epsilon), \quad (50)$$

and the discontinuity condition for the normal derivative,

$$\frac{\psi'(0 - \epsilon)}{m_*} - \frac{\psi'(0 + \epsilon)}{m} = \frac{2}{\hbar^2} (\mathcal{W} \pm \tilde{\alpha} k_{\parallel}) \psi(0), \quad (51)$$

where  $\epsilon \rightarrow 0+$ . For the bulk states I and II, the junction conditions (50,51) do not determine the wave numbers  $k_i$ , but only the ratios of the expansion coefficients; e.g., for a free

state ( $k_i > \sqrt{2m\Phi}/\hbar$ )

$$\begin{aligned} \psi_{k_i, k_{\parallel}}(z) = & F(k_i, k_{\parallel})[\Theta(z) \exp(ik_z z) \\ & + \Theta(-z)A(k_i, k_{\parallel}) \exp(ik_i z) \\ & + \Theta(-z)B(k_i, k_{\parallel}) \exp(-ik_i z)], \end{aligned} \quad (52)$$

or for a bound state ( $0 < k_i < \sqrt{2m\Phi}/\hbar$ )

$$\begin{aligned} \psi_{k_i, k_{\parallel}}(z) = & F(k_i, k_{\parallel})[\Theta(z) \exp(-\kappa z) \\ & + \Theta(-z)A(k_i, k_{\parallel}) \exp(ik_i z) \\ & + \Theta(-z)B(k_i, k_{\parallel}) \exp(-ik_i z)]. \end{aligned} \quad (53)$$

Thus, these states will not exhibit the Rashba spin splitting of energy bands, contrary to the 2D electron gas of interface states III, where the junction conditions completely determine the damping coefficients and hence the energy bands in terms of  $\mathcal{W}$ ,  $\tilde{\alpha}$  and  $k_{\parallel}$ .

### A. Interface states in the asymmetric model

The interface states are

$$\begin{aligned} \psi_{k_{\parallel}, \pm}(z) = & \langle z | k_{\parallel}, \pm \rangle \\ = & \sqrt{\frac{2\kappa_{\pm}\kappa_{i, \pm}}{\kappa_{\pm} + \kappa_{i, \pm}}} [\Theta(z) \exp(-\kappa_{\pm} z) + \Theta(-z) \exp(\kappa_{i, \pm} z)], \end{aligned} \quad (54)$$

with the damping coefficients,

$$\begin{aligned} \kappa_{\pm} = & -\frac{2mm_*}{\hbar^2} \frac{\mathcal{W} \pm \tilde{\alpha}k_{\parallel}}{m - m_*} \\ & + \left[ \frac{4m^3 m_*}{\hbar^4} \left( \frac{\mathcal{W} \pm \tilde{\alpha}k_{\parallel}}{m - m_*} \right)^2 + \frac{2m^2 \Phi}{\hbar^2(m - m_*)} - \frac{m}{m_*} k_{\parallel}^2 \right]^{\frac{1}{2}}, \end{aligned} \quad (55)$$

$$\begin{aligned} \kappa_{i, \pm} = & \frac{2mm_*}{\hbar^2} \frac{\mathcal{W} \pm \tilde{\alpha}k_{\parallel}}{m - m_*} \\ & - \left[ \frac{4mm_*^3}{\hbar^4} \left( \frac{\mathcal{W} \pm \tilde{\alpha}k_{\parallel}}{m - m_*} \right)^2 + \frac{2m_*^2 \Phi}{\hbar^2(m - m_*)} - \frac{m_*}{m} k_{\parallel}^2 \right]^{\frac{1}{2}} \end{aligned} \quad (56)$$

if  $m > m_*$ , and

$$\begin{aligned} \kappa_{\pm} = & \frac{2mm_*}{\hbar^2} \frac{\mathcal{W} \pm \tilde{\alpha}k_{\parallel}}{m_* - m} \\ & - \left[ \frac{4m^3 m_*}{\hbar^4} \left( \frac{\mathcal{W} \pm \tilde{\alpha}k_{\parallel}}{m_* - m} \right)^2 - \frac{2m^2 \Phi}{\hbar^2(m_* - m)} - \frac{m}{m_*} k_{\parallel}^2 \right]^{\frac{1}{2}}, \end{aligned} \quad (57)$$

$$\begin{aligned} \kappa_{i, \pm} = & -\frac{2mm_*}{\hbar^2} \frac{\mathcal{W} \pm \tilde{\alpha}k_{\parallel}}{m_* - m} \\ & + \left[ \frac{4mm_*^3}{\hbar^4} \left( \frac{\mathcal{W} \pm \tilde{\alpha}k_{\parallel}}{m_* - m} \right)^2 - \frac{2m_*^2 \Phi}{\hbar^2(m_* - m)} - \frac{m_*}{m} k_{\parallel}^2 \right]^{\frac{1}{2}} \end{aligned} \quad (58)$$

if  $m < m_*$ .

The “-” branch is again restricted by the requirement  $\mathcal{W} - \tilde{\alpha}k_{\parallel} > 0$ , which follows from  $\kappa_{i, -} > 0$  if  $m > m_*$ , or from  $\kappa_{-, -} > 0$  if  $m < m_*$ . Furthermore, the requirements  $\kappa_{\pm} > 0$  and  $\kappa_{i, \pm} > 0$  also imply for  $m \geq m_*$  the conditions,

$$\begin{aligned} \Phi - \frac{2m}{\hbar^2} (\mathcal{W} \pm \tilde{\alpha}k_{\parallel})^2 < & \hbar^2 k_{\parallel}^2 \frac{m - m_*}{2mm_*} \\ < \Phi + \frac{2m_*}{\hbar^2} (\mathcal{W} \pm \tilde{\alpha}k_{\parallel})^2, \end{aligned} \quad (59)$$

while the conditions for  $m \leq m_*$  are

$$\Phi + \hbar^2 k_{\parallel}^2 \frac{m_* - m}{2mm_*} < \frac{2m}{\hbar^2} (\mathcal{W} \pm \tilde{\alpha}k_{\parallel})^2. \quad (60)$$

Note that these are different constraints for the two Rashba spin-split dispersion relations,

$$E_{\pm}(k_{\parallel}) \equiv E(k_{\parallel}, \kappa_{i, \pm}(k_{\parallel})) = \frac{\hbar^2}{2m_*} (k_{\parallel}^2 - \kappa_{i, \pm}^2), \quad (61)$$

where the inner-cone dispersion  $E_{-}(k_{\parallel}) \geq E_{+}(k_{\parallel})$  has a tighter constraint. The outer-cone dispersion  $E_{+}(k_{\parallel})$  will always persist for larger momentum ranges than  $E_{-}(k_{\parallel})$ , thus always favoring the Edelstein charge-spin conversion effects.

The general expressions are rather unwieldy. Therefore let us look at the case  $m = m_*$  in more detail. The solutions for the damping coefficients in this case reduce to

$$\kappa_{\pm} = \frac{m}{\hbar^2} (\mathcal{W} \pm \tilde{\alpha}k_{\parallel}) + \frac{\Phi}{2(\mathcal{W} \pm \tilde{\alpha}k_{\parallel})}, \quad (62)$$

$$\kappa_{i, \pm} = \frac{m}{\hbar^2} (\mathcal{W} \pm \tilde{\alpha}k_{\parallel}) - \frac{\Phi}{2(\mathcal{W} \pm \tilde{\alpha}k_{\parallel})}, \quad (63)$$

while the conditions (59) or (60) reduce with  $\mathcal{W} \pm \tilde{\alpha}k_{\parallel} > 0$  (which follows from  $\kappa_{\pm} > 0$ ) to

$$\mathcal{W} \pm \tilde{\alpha}k_{\parallel} > \hbar \sqrt{\frac{\Phi}{2m}}. \quad (64)$$

For the interface energy band  $E_{+}(k_{\parallel})$ , this implies

$$k_{\parallel} > \frac{1}{\tilde{\alpha}} \left( \hbar \sqrt{\frac{\Phi}{2m}} - \mathcal{W} \right), \quad (65)$$

which provides a lower cutoff only if  $\Phi > 2m\mathcal{W}^2/\hbar^2$ , as  $\kappa_{i, +} > 0$  would not hold for smaller values of  $k_{\parallel}$ . Since  $\kappa_{i, +} = 0$  for the lower bound in Eq. (64), the minimum energy for  $E_{+}(k_{\parallel})$  in this case is

$$E_{+}(k_{\parallel}) > \frac{\hbar^2}{2m\tilde{\alpha}^2} \left( \hbar \sqrt{\frac{\Phi}{2m}} - \mathcal{W} \right)^2. \quad (66)$$

This appearance of a minimum cutoff for the interface momentum and energy band may seem surprising at the first sight, but can be understood as a consequence of the  $k_{\parallel}$ -dependent enhancement of the attractive interface potential in the  $E_{+}(k_{\parallel})$  branch:  $\mathcal{W} \rightarrow \mathcal{W} + \tilde{\alpha}k_{\parallel}$ . An attractive  $\delta$  potential at a potential step of height  $\Phi$  cannot support a bound state if the step is too high,  $\Phi > 2m\mathcal{W}^2/\hbar^2$ . However, the spin-orbit coupling enhances the effect of the attractive potential in the  $E_{+}(k_{\parallel})$  branch, and therefore can reestablish the bound state if the enhancement is strong enough. Since the effect is linear in  $k_{\parallel}$ , we have the conditions (65,66) for the existence of interface states in the presence of a large potential step.

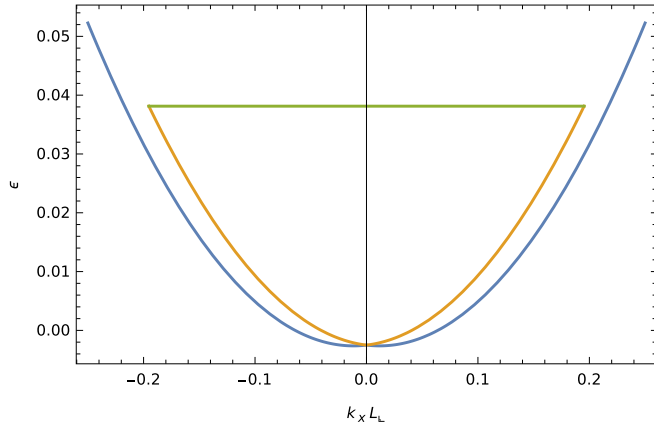


FIG. 9. The spin-split interface energy bands  $\epsilon_{\pm} = (2mL_{\perp}^2/\hbar^2)E_{\pm}$  as a function of  $k_x L_{\perp}$  for  $k_y = 0$  and for weak asymmetry,  $\gamma < 2\beta^2$ . The blue (orange) curve corresponds to  $E_+$  ( $E_-$ ) in Eq. (61). Due to the requirement  $\kappa_{i,-} > 0$ ,  $\epsilon_-$  is restricted to a maximum value of  $(\beta - \sqrt{\gamma/2})^2/\eta^2$ . The cutoff is indicated by the green line. Here,  $\beta = 0.1$ ,  $\gamma = 0.01$ , and  $\eta = 0.15$ .

For the interface energy band  $E_-(k_{\parallel})$ , condition (64) implies

$$k_{\parallel} < \frac{1}{\tilde{\alpha}} \left( \mathcal{W} - \hbar \sqrt{\frac{\Phi}{2m}} \right), \quad (67)$$

which generalizes the condition found earlier for  $\Phi = 0$ . We also note that if  $E_+(k_{\parallel})$  is restricted at all, i.e., if  $\Phi > 2m\mathcal{W}^2/\hbar^2$  holds and (65) must be satisfied, then the inner-cone energy band  $E_-(k_{\parallel})$  is eliminated completely. Again, this can be understood through the effective modification of the interface potential through the spin-orbit coupling. For the  $E_-(k_{\parallel})$  branch, the effective modification  $\mathcal{W} \rightarrow \mathcal{W} - \tilde{\alpha}k_{\parallel}$  further weakens the attractive potential and thus cannot help with creating an interface band. This  $k_{\parallel}$ -dependent weakening of the attractive potential in the  $E_-(k_{\parallel})$  branch also explains termination of the  $E_-(k_{\parallel})$  band for large  $k_{\parallel}$  in the case  $\Phi < 2m\mathcal{W}^2/\hbar^2$ .

In addition to the parameters (28) and (29) we also use the dimensionless parameter,

$$\gamma = \frac{m\Phi L_{\perp}^2}{\hbar^2} = 0.131 \times \frac{m}{m_e} \times \frac{\Phi}{\text{eV}} \times \left( \frac{L_{\perp}}{\text{\AA}} \right)^2, \quad (68)$$

for the asymmetric embedding of the Rashba interface.

We have found that the case  $\Phi < 2m\mathcal{W}^2/\hbar^2$  ( $\gamma < 2\beta^2$ ) behaves qualitatively like the symmetric case  $\Phi = 0$  discussed above. We can therefore label the case  $\gamma < 2\beta^2$  as *weak asymmetry* across the RSOC interface or layer. This is illustrated in Fig. 9.

On the other hand, if we increase the asymmetry so that  $\Phi > 2m\mathcal{W}^2/\hbar^2$  ( $\gamma > 2\beta^2$ ), only the  $E_+(k_{\parallel})$  band of interface states exists. We will see in Sec. VI that it emerges from a band of bound states (case II in Table I). This defines a regime of *strong asymmetry* across the RSOC interface. The corresponding energy band of interface states is illustrated in Fig. 10.

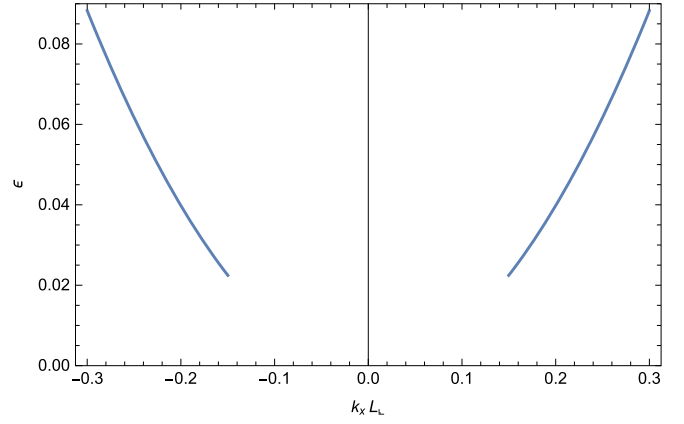


FIG. 10. The interface energy band  $\epsilon_+ = (2mL_{\perp}^2/\hbar^2)E_+$  as a function of  $k_x L_{\perp}$  for  $k_y = 0$  and for strong asymmetry,  $\gamma > 2\beta^2$ . The requirement  $\kappa_{i,+} > 0$  restricts the in-plane momentum for the interface states to  $k_{\parallel} L_{\perp} > (\sqrt{\gamma/2} - \beta)/\eta$ . Here,  $\beta = 0.1$ ,  $\gamma = 0.03$ , and  $\eta = 0.15$ .

## B. Bulk bound states in the asymmetric model

The states referred to as case II in Table I are with  $m = m_*$  given by

$$\begin{aligned} \psi_{k_{\parallel}, k_i, \pm}^{(b)}(z) &= \langle z | k_{\parallel}, k_i, \pm \rangle_b \\ &= F_{b,\pm}(k_i, k_{\parallel}) [\Theta(z) \exp(-\kappa z) \\ &\quad + \Theta(-z) A_{b,\pm}(k_i, k_{\parallel}) \exp(ik_i z) \\ &\quad + \Theta(-z) A_{b,\pm}^*(k_i, k_{\parallel}) \exp(-ik_i z)], \end{aligned} \quad (69)$$

where

$$k_i^2 = \frac{2m\Phi}{\hbar^2} - \kappa^2, \quad (70)$$

$$A_{b,\pm}(k_i, k_{\parallel}) = \frac{1}{2} - i \frac{(2m/\hbar^2)(\mathcal{W} \pm \tilde{\alpha}k_{\parallel}) - \sqrt{(2m\Phi/\hbar^2) - k_i^2}}{2k_i}, \quad (71)$$

and

$$F_{b,\pm}(k_i, k_{\parallel}) = \frac{1}{\sqrt{2\pi} |A_{b,\pm}(k_i, k_{\parallel})|}. \quad (72)$$

## C. Free states in the asymmetric model

The free states (case I in Table I) are with  $m = m_*$  given by

$$\begin{aligned} \psi_{k_{\parallel}, k_i, \pm}^{(f)}(z) &= \langle z | k_{\parallel}, k_i, \pm \rangle_f \\ &= F_{f,\pm}(k_i, k_{\parallel}) [\Theta(z) \exp(ik_z z) \\ &\quad + \Theta(-z) A_{f,\pm}(k_i, k_{\parallel}) \exp(ik_i z) \\ &\quad + \Theta(-z) B_{f,\pm}(k_i, k_{\parallel}) \exp(-ik_i z)], \end{aligned} \quad (73)$$

where

$$k_i^2 = \frac{2m\Phi}{\hbar^2} + k_z^2, \quad (74)$$

$$A_{f,\pm}(k_i, k_{\parallel}) = \frac{1}{2} + \frac{\sqrt{k_i^2 - (2m\Phi/\hbar^2)} - i(2m/\hbar^2)(\mathcal{W} \pm \tilde{\alpha}k_{\parallel})}{2k_i}, \quad (75)$$

$$B_{f,\pm}(k_i, k_{\parallel}) = \frac{1}{2} \frac{\sqrt{k_i^2 - (2m\Phi/\hbar^2) - i(2m/\hbar^2)(\mathcal{W} \pm \tilde{\alpha}k_{\parallel})}}{2k_i}, \quad (76)$$

and

$$F_{f,\pm}(k_i, k_{\parallel}) = \frac{1}{\sqrt{\pi}} \left[ \frac{k_z(k_i)}{k_i} + |A_{f,\pm}(k_i, k_{\parallel})|^2 + |B_{f,\pm}(k_i, k_{\parallel})|^2 \right]^{-1/2}. \quad (77)$$

## VI. DENSITIES OF STATES IN THE ASYMMETRIC MODEL

We indicate the full three-dimensional states through bold-face notation for the momentum parallel to the interface. Namely, the interface states are  $|\mathbf{k}_{\parallel}, \pm\rangle = |\mathbf{k}_{\parallel}\rangle \otimes |k_{\parallel}, \pm\rangle \otimes |\varphi_{\pm}(\mathbf{k}_{\parallel})\rangle$ , while the bound and free states are  $|\mathbf{k}_{\parallel}, k_i, \pm\rangle = |\mathbf{k}_{\parallel}\rangle \otimes |k_{\parallel}, k_i, \pm\rangle \otimes |\varphi_{\pm}(\mathbf{k}_{\parallel})\rangle$ , where  $|\mathbf{k}_{\parallel}\rangle$  are the plane-wave states for motion parallel to the interface and  $|\varphi_{\pm}(\mathbf{k}_{\parallel})\rangle$  are the chiral spin-momentum-locked states with components  $\varphi_{\pm,a}(\mathbf{k}_{\parallel})$  given by Eq. (13).

The states are normalized to (with  $s, s' \in \{+, -\}$ )

$$\langle \mathbf{k}_{\parallel}, s | \mathbf{k}'_{\parallel}, s' \rangle = \delta_{s,s'} \delta(\mathbf{k}_{\parallel} - \mathbf{k}'_{\parallel}), \quad (78)$$

$$\langle \mathbf{k}_{\parallel}, s | \mathbf{k}'_{\parallel}, k_i, s' \rangle = 0, \quad (79)$$

and

$$\langle \mathbf{k}_{\parallel}, k_i, s | \mathbf{k}'_{\parallel}, k'_i, s' \rangle = \delta_{s,s'} \delta(\mathbf{k}_{\parallel} - \mathbf{k}'_{\parallel}) \delta(k_i - k'_i). \quad (80)$$

Note that the factor  $\delta(\mathbf{k}_{\parallel} - \mathbf{k}'_{\parallel}) = \langle \mathbf{k}_{\parallel} | \mathbf{k}'_{\parallel} \rangle$  originates in the plane-wave states, and the presence of this factor in turn implies the factors  $\delta_{s,s'} = \langle \varphi_s(\mathbf{k}_{\parallel}) | \varphi_{s'}(\mathbf{k}_{\parallel}) \rangle$ . The remaining parts of the relations can then be verified using the well-known relations,

$$\int_{-\infty}^0 dz \exp[i(k - i\varepsilon)z] = \pi \delta(k) - i\mathcal{P} \frac{1}{k}, \quad (81)$$

$$\int_0^{\infty} dz \exp[i(k + i\varepsilon)z] = \pi \delta(k) + i\mathcal{P} \frac{1}{k}. \quad (82)$$

The completeness relation for the states is

$$\begin{aligned} & \int d^2 \mathbf{k}_{\parallel} \left[ \Theta(\beta - \sqrt{\gamma/2} - \eta L_{\perp} k_{\parallel}) |\mathbf{k}_{\parallel}, -\rangle \langle \mathbf{k}_{\parallel}, -| \right. \\ & + \Theta(\beta - \sqrt{\gamma/2} + \eta L_{\perp} k_{\parallel}) |\mathbf{k}_{\parallel}, +\rangle \langle \mathbf{k}_{\parallel}, +| \\ & + \int_0^{\sqrt{2m\Phi/\hbar}} dk_i \sum_{s \in \{+, -\}} |\mathbf{k}_{\parallel}, k_i, s\rangle_b \langle \mathbf{k}_{\parallel}, k_i, s| \\ & \left. + \int_{\sqrt{2m\Phi/\hbar}}^{\infty} dk_i \sum_{s \in \{+, -\}} |\mathbf{k}_{\parallel}, k_i, s\rangle_f \langle \mathbf{k}_{\parallel}, k_i, s| \right] \\ & = 1. \end{aligned} \quad (83)$$

The Heaviside functions take into account that the momentum ranges for the interface states in the left- or right-chiral sector are limited if  $\beta > \sqrt{\gamma/2}$  or  $\beta < \sqrt{\gamma/2}$ , respectively.

The completeness relation can be verified through confirmation that the matrix elements of LHS in the Fourier basis  $|\mathbf{k}, \sigma\rangle = |\mathbf{k}\rangle \otimes |\sigma\rangle$  yields  $\delta(\mathbf{k} - \mathbf{k}') \delta_{\sigma,\sigma'}$ . Here  $|\mathbf{k}\rangle$  are the three-dimensional plane-wave states and  $|\sigma\rangle$ ,  $\sigma \in \{\uparrow, \downarrow\}$ , are the standard spinors of the Pauli matrices.

### A. Densities of interface states

We continue to use the dimensionless energy variable  $\epsilon = 2mL_{\perp}^2 E/\hbar^2$  for the DOS. The energies of the right- and left-chiral interface states are then with  $\xi \equiv k_{\parallel} L_{\perp}$ ,

$$\epsilon_{\pm}(\xi) = \xi^2 - \left( \beta \pm \eta \xi - \frac{\gamma}{2(\beta \pm \eta \xi)} \right)^2. \quad (84)$$

Due to the condition (67), left-chiral interface states contribute to the local density of states only if the asymmetry is not too large,  $\sqrt{\gamma/2} < \beta$ , and for energy values  $-\beta - (\gamma/2\beta)]^2 \leq \epsilon \leq \eta^{-2}[\beta - \sqrt{\gamma/2}]^2$ . The contribution from the left-chiral interface states is thus

$$\begin{aligned} \varrho_{-}(E, \mathbf{x}) &= \frac{1}{2\pi} \Theta(\beta - \sqrt{\gamma/2}) k_{\parallel}(E) |dk_{\parallel}(E)/dE| \\ & \times |\langle z | k_{\parallel}(E), - \rangle|^2, \end{aligned} \quad (85)$$

where  $k_{\parallel}(E)$  is the solution to  $\epsilon_{-}(k_{\parallel} L_{\perp}) = 2mL_{\perp}^2 E/\hbar^2$ . This solution is unique due to  $\epsilon'_{-}(\xi) > 0$ . The trivial contributions from the plane waves and spin factors have already been evaluated in this expression.

The contribution from the right-chiral interface states is

$$\begin{aligned} \varrho_{+}(E, \mathbf{x}) &= \frac{1}{2\pi} \Theta(\beta - \sqrt{\gamma/2}) \Theta(-\epsilon - [\beta - (\gamma/2\beta)]^2) \\ & \times \sum_{(\pm)} k_{\parallel}^{(\pm)}(E) \left| \frac{dk_{\parallel}^{(\pm)}(E)}{dE} \right| |\langle z | k_{\parallel}^{(\pm)}(E), + \rangle|^2 \\ & + \frac{1}{2\pi} \Theta(\epsilon + [\beta - (\gamma/2\beta)]^2) \\ & \times k_{\parallel}(E) |dk_{\parallel}(E)/dE| |\langle z | k_{\parallel}(E), + \rangle|^2, \end{aligned} \quad (86)$$

where  $k_{\parallel}^{(\pm)}(E)$  are the two roots of the condition  $\epsilon_{\pm}(k_{\parallel} L_{\perp}) = 2mL_{\perp}^2 E/\hbar^2$  in the energy range  $\epsilon \leq -[\beta - (\gamma/2\beta)]^2$ , which is accessible only in the weakly asymmetric case.

The primary novel feature of the asymmetric case is the emergence of a single interface energy band with the right chirality at finite energy (66),  $\epsilon_{+} \geq \eta^{-2}(\sqrt{\gamma/2} - \beta)^2$ , in the strongly asymmetric case  $\gamma > 2\beta^2$ . Figure 11 presents such an example.

### B. Densities of free states

The densities of free states in the two chiral sectors are

$$\begin{aligned} \varrho_{f\pm}(E, \mathbf{x}) &= \frac{1}{2\pi} \int_0^{\sqrt{2m(E-\Phi)/\hbar}} dk_{\parallel} k_{\parallel} \left| \frac{\partial k_i(k_{\parallel}, E)}{\partial E} \right| \\ & \times |\langle z | k_{\parallel}, k_i(k_{\parallel}, E), \pm \rangle_f|^2, \end{aligned} \quad (87)$$

respectively, and the ‘‘internal’’ momenta in the  $z$  direction are

$$k_i(k_{\parallel}, E) = \sqrt{\frac{2mE}{\hbar^2} - k_{\parallel}^2}. \quad (88)$$

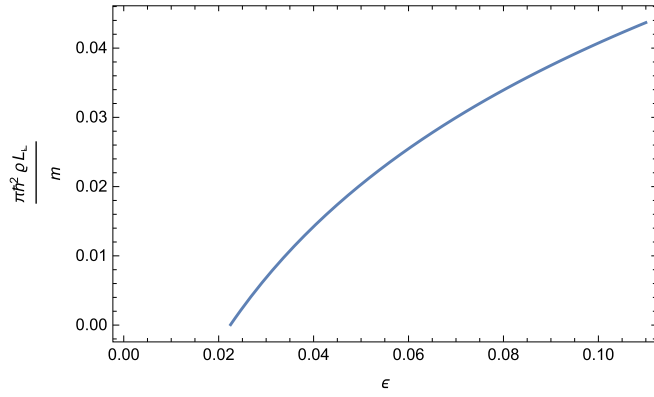


FIG. 11. The density of interface states at  $z = 0$  as a function of energy  $\epsilon = (2mL_{\perp}^2/\hbar^2)E$  and for strong asymmetry,  $\gamma > 2\beta^2$ . Here,  $\beta = 0.1$ ,  $\gamma = 0.03$ , and  $\eta = 0.15$ .

The presence of the potential step across the interface implies an energy threshold for the free states,

$$E > \Phi \quad (\epsilon > 2\gamma). \quad (89)$$

The densities of free states in Eq. (87) at the interface,  $z = 0$ , are shown in Fig. 12.

### C. Densities of bound states

The densities of bound states in the two chiral sectors are

$$\rho_{b\pm}(E, \mathbf{x}) = \frac{1}{2\pi} \int_{\Theta(E-\Phi), \sqrt{2m(E-\Phi)}/\hbar}^{\sqrt{2mE}/\hbar} dk_{\parallel} k_{\parallel} \left| \frac{\partial k_i(k_{\parallel}, E)}{\partial E} \right| |\langle z | k_{\parallel}, k_i(k_{\parallel}, E), \pm \rangle_b|^2, \quad (90)$$

where  $k_i(k_{\parallel}, E)$  is still given by Eq. (88), but now  $k_i^2 < 2m\Phi/\hbar^2$ . This leads to the constraint,

$$k_{\parallel} \geq \Theta(E - \Phi) \sqrt{2m(E - \Phi)}/\hbar, \quad (91)$$

for the momentum parallel to the RSOC interface. The resulting densities of bound states in Eq. (90) at the interface,  $z = 0$ , in the strongly asymmetric case are presented in Fig. 13.

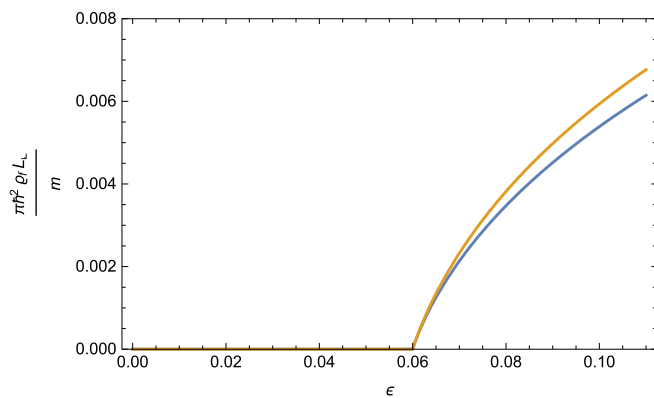


FIG. 12. The density of right- and left-chiral free states as a function of energy  $\epsilon = (2mL_{\perp}^2/\hbar^2)E$ . The blue (orange) curve corresponds to  $\rho_{f+}$  ( $\rho_{f-}$ ) in Eq. (87) and in the interface,  $z = 0$ . Here,  $\beta = 0.1$ ,  $\gamma = 0.03$ , and  $\eta = 0.15$ .

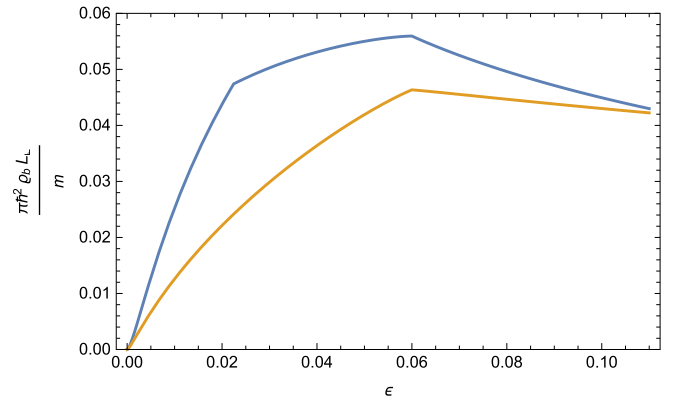


FIG. 13. The density of right- and left-chiral bound states as a function of energy  $\epsilon = (2mL_{\perp}^2/\hbar^2)E$  in the case of strong asymmetry across the interface. The blue (orange) curve corresponds to  $\rho_{b+}$  ( $\rho_{b-}$ ) in Eq. (90) and in the interface,  $z = 0$ . Here,  $\beta = 0.1$ ,  $\gamma = 0.03$ , and  $\eta = 0.15$ .

As expected from our observation of thresholds in the interface and free states, the density of right-chiral bound states  $\rho_{b+}$  shows cusps at the thresholds,

$$\epsilon_{i,+} = \frac{1}{\eta^2} \left( \sqrt{\frac{\gamma}{2}} - \beta \right)^2, \quad (92)$$

for the onset of interface states in the presence of strong asymmetry, and

$$\epsilon_{f,\pm} = 2\gamma \quad (93)$$

for the onset of free states, whereas  $\rho_{b-}$  only has a cusp at the threshold (93). Note that  $\epsilon_{i,+} < \epsilon_{f,\pm} \Leftrightarrow \eta > 0.5 - (\beta/\sqrt{2\gamma})$ .

The threshold (93) is manifestly visible in the lower bound of the integral in Eq. (90). However, the threshold (92) arises in  $\rho_{b+}(E)$  from the contribution near the upper bound. The integrand near the upper bound vanishes as  $(\sqrt{\epsilon} - \xi)^{1/2}$  for generic values of  $\epsilon$ , but for right-chiral states diverges as  $(\sqrt{\epsilon} - \xi)^{-1/2}$  at the threshold value (92). The total densities

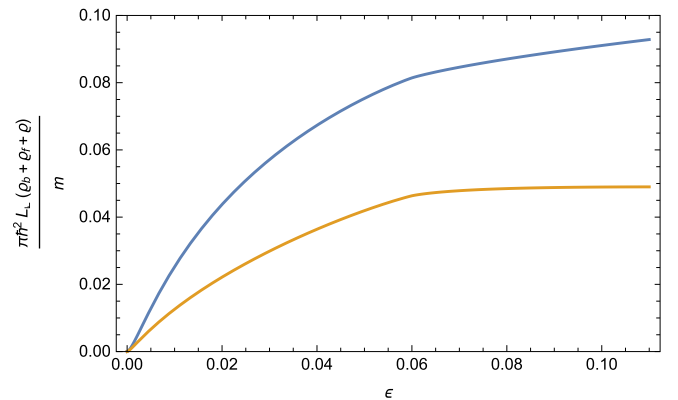


FIG. 14. The total density of right- and left-chiral states as a function of energy  $\epsilon = (2mL_{\perp}^2/\hbar^2)E$  in the case of strong asymmetry across the interface. The blue (orange) curve corresponds to  $\rho_{b+} + \rho_{f+} + \rho_{b-} + \rho_{f-}$  in the interface,  $z = 0$ . Here,  $\beta = 0.1$ ,  $\gamma = 0.03$ , and  $\eta = 0.15$ .

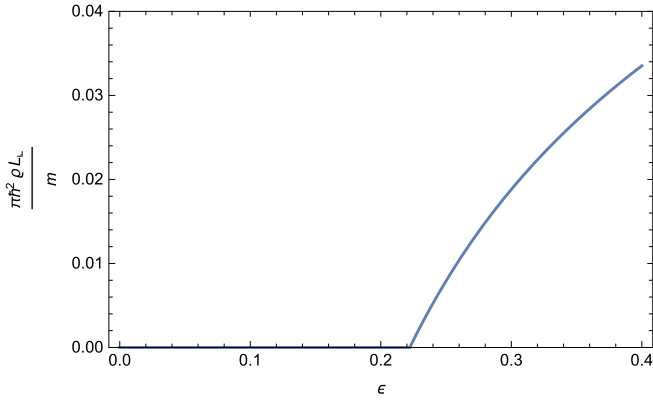


FIG. 15. The density of interface states at  $z = 0$  as a function of energy  $\epsilon = (2mL_{\perp}^2/\hbar^2)E$  and for  $\beta = 0$ . Here,  $\gamma = 0.01$  and  $\eta = 0.15$ .

of right- and left-chiral states are smooth, although the second derivatives change at the critical value (93), see Fig. 14.

The right-chiral states continue to dominate in the “3D+2D” models, although for the contributions from the bound and free states, this is a consequence of “spin-split wave functions” entering the local densities of states through  $|\langle z|k_{\parallel}, k_{\perp}(k_{\parallel}, E), \pm\rangle|^2$ , instead of spin-split energy bands themselves. The spin-charge correlation through the (inverse) Edelstein effect is therefore also maintained in the “3D+2D” models.

#### D. Densities of states for $V_0 = 0$

As mentioned in Sec. II, the case  $V_0 = \mathcal{W}/L_{\perp} = 0$  may be of special interest for metallic interfaces. In this case, the subdominant inner interface band ( $E_{-}(k_{\parallel})$  for  $\alpha > 0$ ) is always suppressed, and we have the threshold  $k_{\parallel}L_{\perp} > \eta^{-1}\sqrt{\gamma/2}$ ,  $\epsilon_{+} > \gamma/2\eta^2$  for the dominant outer interface energy band. Corresponding densities of interface states, free states, and bound states are illustrated in Figs. 15–17, respectively. Figure 16 shows only one curve because the densities of right- and left-chiral free states in the interface are identical for

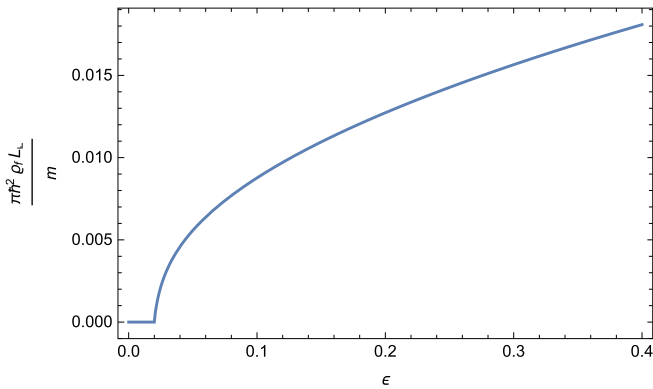


FIG. 16. The density of right- and left-chiral free states as a function of energy  $\epsilon = (2mL_{\perp}^2/\hbar^2)E$  for  $\beta = 0$  and in the interface,  $z = 0$ . In this case, we have  $\rho_{f+} = \rho_{f-}$ , since the corresponding wave functions only differ in phase. Here,  $\gamma = 0.01$  and  $\eta = 0.15$ .

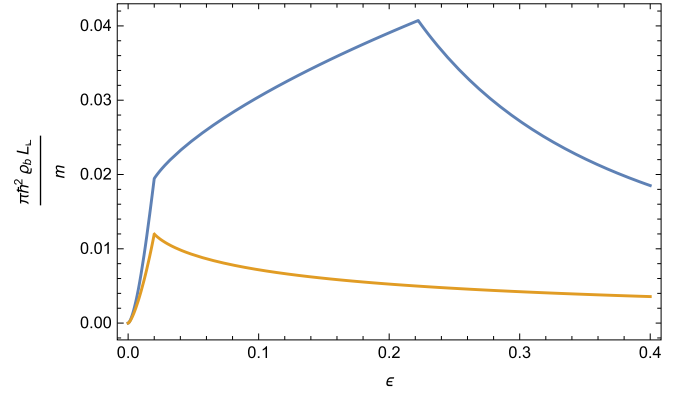


FIG. 17. The density of right- and left-chiral bound states as a function of energy  $\epsilon = (2mL_{\perp}^2/\hbar^2)E$  for  $\beta = 0$ . The blue (orange) curve corresponds to  $\rho_{b+}$  ( $\rho_{b-}$ ) in Eq. (90) and in the interface,  $z = 0$ . Here,  $\gamma = 0.01$  and  $\eta = 0.15$ .

$\beta = 0$ . The sums of all three partial densities of states are again smooth in both chiral sectors, as can be seen in Fig. 18.

## VII. CONCLUSIONS

We have constructed model Hamiltonians for electrons in three-dimensional systems with two-dimensional substructure such as a surface or an interface, in which the electrons experience Rashba spin-orbit coupling. We have obtained analytic results for the wave functions and densities of states at the location of the interface. In the case of weak asymmetry across the interface, there are two spin-split energy bands of interface states,  $E_{+}(\mathbf{k}_{\parallel})$  and  $E_{-}(\mathbf{k}_{\parallel})$ , just like in the two-dimensional Bychkov-Rashba model [6]. However, if the in-plane momentum  $k_{\parallel} = |\mathbf{k}_{\parallel}|$  increases beyond a critical value, the subdominant interface band (the left-chiral band  $E_{-}(\mathbf{k}_{\parallel})$  for  $\alpha > 0$ ) is absorbed into a bulk energy band due to the effective weakening of the attractive potential with  $V_0 - |\alpha|k_{\parallel}$ . In the case of strong asymmetry across the interface, there is only one energy band of interface states (the right-chiral band  $E_{+}(\mathbf{k}_{\parallel})$  for  $\alpha > 0$ ) emerging from a bulk energy band

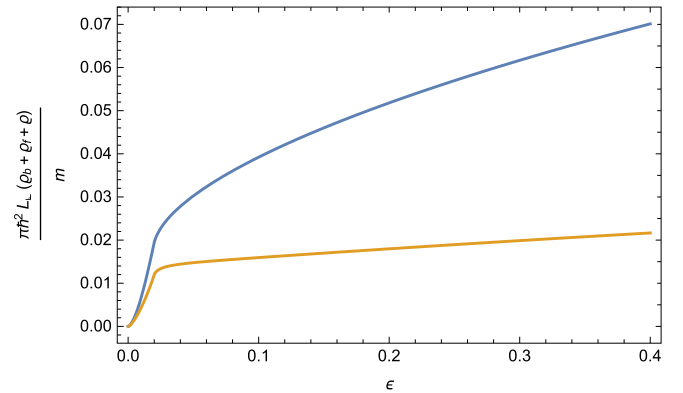


FIG. 18. The total density of right- and left-chiral bound states as a function of energy  $\epsilon = (2mL_{\perp}^2/\hbar^2)E$  for  $\beta = 0$ . The blue (orange) curve corresponds to  $\rho_{b+} + \rho_{b-} + \rho_{f+}$  ( $\rho_{b-} + \rho_{f-}$ ) in the interface,  $z = 0$ . Here,  $\gamma = 0.01$  and  $\eta = 0.15$ .

if  $k_{\parallel}$  increases beyond a critical value, due to the effective strengthening of the attractive interface potential with  $V_0 + |\alpha|k_{\parallel}$ .

The total density of bulk + interface states is always dominated by the right chirality for  $\alpha > 0$  (or the left chirality for  $\alpha < 0$ ), just like in the two-dimensional Bychkov-Rashba model. Thus, the “3D+2D” models studied in this work support the (inverse) Edelstein charge-spin correlation effects. However, for the contributions from the bulk bands, this is not a consequence of spin-split energy bands,

but of a larger weight of the wave functions of the preferred chirality.

## ACKNOWLEDGMENTS

This research was supported by the Natural Sciences and Engineering Research Council of Canada. We thank Frank Marsiglio for enlightening discussions and referees for constructive criticisms, which have helped us to improve the manuscript.

- 
- [1] R. Dick, *Physica E* **40**, 2973 (2008); *Nanoscale Res. Lett.* **5**, 1546 (2010).
- [2] R. Dick, *Nanoscale Res. Lett.* **7**, 581 (2012).
- [3] R. Dick, *Advanced Quantum Mechanics: Materials and Photons*, 2nd ed. (Springer Nature, 2016).
- [4] E. I. Rashba, *Sov. Phys. Solid State* **1**, 368 (1959); **2**, 1109 (1960).
- [5] R. C. Casella, *Phys. Rev. Lett.* **5**, 371 (1960).
- [6] Yu. A. Bychkov and E. I. Rashba, *JETP Lett.* **39**, 78 (1984).
- [7] R. Winkler, *Spin-Orbit Coupling Effects in Two-Dimensional Electron and Hole Systems* (Springer, Berlin, 2003).
- [8] S. A. Wolf, D. D. Awschalom, R. A. Buhrman, J. M. Daughton, S. von Molnár, M. L. Roukes, A. Y. Chtchelkanova, and D. M. Treger, *Science* **294**, 1488 (2001); I. Zutic, J. Fabian, and S. Das Sarma, *Rev. Mod. Phys.* **76**, 323 (2004).
- [9] A. Soumyanarayanan, N. Reyren, A. Fert, and C. Panagopoulos, *Nature (London)* **539**, 509 (2016).
- [10] Y. Kunihashi, T. Nihei, M. Kohda, and J. Nitta, *Phys. Stat. Sol. (c)* **5**, 322 (2008).
- [11] M. Nishioka, B. A. Gurney, E. E. Marinero, and F. Mireles, *Appl. Phys. Lett.* **95**, 242108 (2009).
- [12] A. Violante, R. Hey, and P. V. Santos, *Phys. Rev. B* **91**, 125302 (2015); S. Souma, A. Sawada, H. Chen, Y. Sekine, M. Eto, and T. Koga, *Phys. Rev. Appl.* **4**, 034010 (2015).
- [13] Won Young Choi, Hyung-jun Kim, Joonyeon Chang, Gyungchoon Go, Kyung-Jin Lee, and Hyun Cheol Koo, *Curr. Appl. Phys.* **17**, 513 (2017).
- [14] P. D. C. King, R. C. Hatch, M. Bianchi, R. Ovsyannikov, C. Lupulescu, G. Landolt, B. Slomski, J. H. Dil, D. Guan, J. L. Mi, E. D. L. Rienks, J. Fink, A. Lindblad, S. Svensson, S. Bao, G. Balakrishnan, B. B. Iversen, J. Osterwalder, W. Eberhardt, F. Baumberger, and Ph. Hofmann, *Phys. Rev. Lett.* **107**, 096802 (2011); V. Gnezdilov, P. Lemmens, D. Wulferding, A. Möller, P. Recher, H. Berger, R. Sankar, and F. C. Chou, *Phys. Rev. B* **89**, 195117 (2014); P. Moras, G. Bihlmayer, P. M. Sheverdyaeva, S. K. Mahatha, M. Papagno, J. Sánchez-Barriga, O. Rader, L. Novinec, S. Gardonio, and C. Carbone, *ibid.* **91**, 195410 (2015).
- [15] O. J. Clark, F. Mazzola, J. Feng, V. Sunko, I. Marković, L. Bawden, T. K. Kim, P. D. C. King, and M. S. Bahrmy, *Phys. Rev. B* **99**, 045438 (2019).
- [16] V. M. Edelstein, *Solid State Commun.* **73**, 233 (1990).
- [17] W. Han, Y.-C. Otani, and S. Maekawa, *npj Quantum Mat.* **3**, 27 (2018).
- [18] M. Z. Hasan and C. L. Kane, *Rev. Mod. Phys.* **82**, 3045 (2010); X.-L. Qi and S.-C. Zhang, *ibid.* **83**, 1057 (2011).
- [19] J. C. Rojas Sánchez, L. Vila, G. Desfonds, S. Gambarelli, J. P. Attané, J. M. De Teresa, C. Magén, and A. Fert, *Nat. Comm.* **4**, 2944 (2013); W. Zhang, M. B. Jungfleisch, W. Jiang, J. E. Pearson, and A. Hoffmann, *Appl. Phys.* **117**, 17C727 (2015).
- [20] H. J. Zhang, S. Yamamoto, B. Gu, H. Li, M. Maekawa, Y. Fukaya, and A. Kawasuso, *Phys. Rev. Lett.* **114**, 166602 (2015).
- [21] M. Isasa, M. C. Martínez-Velarte, E. Villamor, C. Magén, L. Morellón, J. M. De Teresa, M. R. Ibarra, G. Vignale, E. V. Chulkov, E. E. Krasovskii, L. E. Hueso, and F. Casanova, *Phys. Rev. B* **93**, 014420 (2016).
- [22] A. Ohtomo and H. Y. Hwang, *Nature (London)* **427**, 423 (2004); S. Okamoto and A. J. Millis, *ibid.* **428**, 630 (2004); G. Herranz, M. Basletić, M. Bibes, C. Carrétéro, E. Tafra, E. Jacquet, K. Bouzehouane, C. Deranlot, A. Hamzić, J.-M. Broto, A. Barthélémy, and A. Fert, *Phys. Rev. Lett.* **98**, 216803 (2007); A. D. Caviglia, M. Gabay, S. Gariglio, N. Reyren, C. Cancellieri, and J.-M. Triscone, *ibid.* **104**, 126803 (2010); J. Mannhart and D. G. Schlom, *Science* **327**, 1607 (2010); S. A. Chambers, *Surf. Sci.* **605**, 1133 (2011); H. Y. Hwang, Y. Iwasa, M. Kawasaki, B. Keimer, N. Nagaosa, and Y. Tokura, *Nat. Mat.* **11**, 103 (2012).
- [23] S. Karube, K. Kondou, and Y.-C. Otani, *Appl. Phys. Expr.* **9**, 033001 (2016); J. Kim, Y.-T. Chen, S. Karube, S. Takahashi, K. Kondou, G. Tatara, and Y.-C. Otani, *Phys. Rev. B* **96**, 140409(R) (2017).
- [24] K. S. Novoselov, A. K. Geim, S. V. Morozov, D. Jiang, M. I. Katsnelson, I. V. Grigorieva, S. V. Dubonos, and A. A. Firsov, *Nature (London)* **438**, 197 (2005); A. H. Castro Neto, F. Guinea, N. M. R. Peres, K. S. Novoselov, and A. K. Geim, *Rev. Mod. Phys.* **81**, 109 (2009); D. S. L. Abergel, V. Apalkov, J. Berashevich, K. Ziegler, and T. Chakraborty, *Adv. Phys.* **59**, 261 (2010).
- [25] G. W. Semenoff, *Phys. Rev. Lett.* **53**, 2449 (1984).
- [26] K. Ishizaka, M. S. Bahrmy, H. Murakawa, M. Sakano, T. Shimojima, T. Sonobe, K. Koizumi, S. Shin, H. Miyahara, A. Kimura, K. Miyamoto, T. Okuda, H. Namatame, M. Taniguchi, R. Arita, N. Nagaosa, K. Kobayashi, Y. Murakami, R. Kumai, Y. Kaneko, Y. Onose, and Y. Tokura, *Nat. Mat.* **10**, 521 (2011).
- [27] S. V. Eremeev, I. A. Nechaev, and E. V. Chulkov, *JETP Lett.* **96**, 437 (2012).
- [28] V. M. Edelstein, *Phys. Rev. Lett.* **75**, 2004 (1995).
- [29] J. Hutchinson, J. E. Hirsch, and F. Marsiglio, *Phys. Rev. B* **97**, 184513 (2018).
- [30] L. van Hove, *Phys. Rev.* **89**, 1189 (1953).

- [31] C. R. Ast, G. Wittich, P. Wahl, R. Vogelgesang, D. Pacilé, M. C. Falub, L. Moreschini, M. Papagno, M. Grioni, and K. Kern, *Phys. Rev. B* **75**, 201401(R) (2007).
- [32] E. Cappelluti, C. Grimaldi, and F. Marsiglio, *Phys. Rev. Lett.* **98**, 167002 (2007); *Phys. Rev. B* **76**, 085334 (2007).
- [33] Zhou Li, L. Covaci and F. Marsiglio, *Phys. Rev. B* **85**, 205112 (2012).
- [34] J. Hutchinson and J. Maciejko, *Phys. Rev. B* **96**, 125304 (2017).
- [35] J. Schliemann and D. Loss, *Phys. Rev. B* **68**, 165311 (2003).